Time dependent source apportionment of submicron organic aerosol for a rural site in an alpine valley using a rolling PMF window

Gang Chen[1*], Yulia Sosedova[1,2*], Francesco Canonaco[1,2], Roman Fröhlich[1], Anna Tobler[1,2], Athanasia Vlachou[1], Kaspar R. Daellenbach[1], Carlo Bozzetti[2], Christoph Hueglin[3], Peter Graf[3], Urs Baltensperger[1], Jay G. Slowik[1], Imad El Haddad[1], and André S.H. Prévôt[1**]

[1]Laboratory of Atmospheric Chemistry, Paul Scherrer Institute, CH-5232 Villigen PSI, Switzerland

[2]Datalystica Ltd., Park innovAARE, CH-5234 Villigen, Switzerland

[3]Empa, Swiss Federal Laboratories for Materials Science and Technology, Laboratory for Air Pollution and Environmental Technology, CH-8600 Dübendorf, Switzerland

~~* G.C. and Y.S. contributed equally to this manuscript~~

~~*~~* ~~-~~*Correspondence to:* ~~-~~André S. H. Prévôt (andre.prevot@psi.ch)

Abstract

We ~~have~~ collected one year of aerosol chemical speciation monitor (ACSM) data in Magadino, a village located in the south of the Swiss Alpine region, ~~which is one of the most polluted areas in Switzerland~~one of Switzerland's most polluted areas. We analysed the mass spectra of organic aerosol (OA) by positive matrix ~~factorization~~ factorisation (PMF) using ~~Source~~ source ~~Finder~~ finder ~~Professional~~ professional (SoFi Pro) to retrieve the origins of OA. Therein, we deployed the rolling algorithm to account for the temporal changes of the source profiles, which is closer to the ~~real world~~measurement. As the ~~first~~ first-ever application of rolling PMF with ME-2 analysis on a yearlong dataset that was collected ~~for~~from a rural ~~cite~~site, we resolved two primary OA factors (traffic-related hydrocarbon-like OA (HOA) and biomass burning OA (BBOA)), one ~~local~~ mass-to-charge ratio (*m/z*) 58 related OA (~~LOA~~58-OA) factor, a less ~~oxidized~~ oxidised oxygenated OA (LO-OOA) factor, and a more ~~oxidized~~ oxidised oxygenated OA (MO-OOA) factor. HOA showed stable contributions to the total OA through the whole year ranging from 8.1~~–~~ to 10.1%, while the contribution of BBOA showed a clear seasonal variation with a range of 8.3–27.4% (highest during winter, lowest during summer) and a yearly average of 17.1%. ~~The OOA was represented by two factors (LO-OOA and MO-OOA) throughout the year.~~ OOA (sum of LO-OOA and MO-OOA) contributed 71.6% of the OA mass, varying from 62.5% (in winter) to 78% (in spring and summer). The uncertainties (σ) for the modelled OA factors (i.e., rotational uncertainty and statistical variability of the sources) varied from ±4% (~~LOA~~58-OA) to a maximum of ± 40% (LO-OOA). Considering th~~e fact that BBOA and LO-OOA (showing influences of biomass burning in winter) had significant contributions to the total OA mass, we suggest a reduction and control of~~at BBOA and LO-OOA (showing influences of biomass burning in winter) had significant contributions to the total OA mass, we suggest reducing and controlling the residential heating as a mitigation strategy for better air quality and lower PM levels in this region and similar locations. In

Appendix A, we conducted a head-to-head comparison between the conventional seasonal PMF analysis and the rolling mechanism. ~~It showed~~We found similar or slightly improved results in terms of mass concentrations, correlations with external tracers and factor profiles of the constrained POA factors. The rolling results show smaller scaled residuals and enhanced correlations between OOA factors and corresponding inorganic salts than those of the seasonal solutions, which was most likely because the rolling PMF analysis can capture the temporal variations of the oxidation processes for OOA ~~sources~~components. Specifically, the time dependent factor profiles of MO-OOA and LO-OOA can well explain the temporal viabilities of two main ions for OOA factors, *m/z* 44 (CO_2^+) and *m/z* 43 (mostly $C_2H_3O^+$). This rolling PMF analysis ~~therefore~~, therefore, provides a more realistic source apportionment (SA) solution~~,~~ with time- dependent OA sources. The rolling results ~~show also~~also show good agreement with offline Aerodyne aerosol mass spectrometer (AMS) SA results from filter samples, except for winter. ~~This~~ The latter discrepancy is likely because the online measurement is capable of capturing the fast oxidation processes of biomass burning sources, in contrast to the 24-hour filter samples. This study demonstrates the strengths of the rolling mechanism and provides a comprehensive criterion list for ACSM users to obtain reproducible SA results, and is a role model for similar analyses of such world-wide available data.

1 Introduction

Atmospheric particulate matter (PM) affects human health and climate. In particular, it influences the radiative balance (IPCC, 2014; von Schneidemesser et al., 2015), reduces visibility (Chow et al., 2002; Horvath, 1993), and negatively affects human health by triggering respiratory and cardiovascular diseases and allergies (Daellenbach et al., 2020; Dockery and Pope, 1994; Mauderly and Chow, 2008; Monn, 2001; Pope and Dockery, 2006; von Schneidemesser et al., 2015). Fine PM exposure strongly correlates with the global mortality

rate. Lelieveld et al. (2015) estimated that outdoor air pollution, mostly $PM_{2.5}$ (PM with an aerodynamic diameter smaller than 2.5 µm), causes 3.3 million premature deaths per year worldwide. Despite ~~of~~ this correlation, different aerosol sources may have strongly different effects on health (Daellenbach et al., 2020). Thus, both climate and health effects are affected by particle chemical composition, which is related to emission sources of primary particles and precursor gases for secondary aerosol (IPCC, 2014; Jacobson et al., 2000; Jacobson, 2001; Lelieveld et al., 2015; Ramanathan et al., 2005).

Organic aerosol (OA) constitutes 20–90% of fine PM (Jimenez et al., 2009; Murphy et al., 2006; Zhang et al., 2007)~~,~~ and contains millions of chemical compounds. Since OA is subject of an extremely complex mixture of chemical constituents, with highly dynamic spatial and temporal (seasonal, diurnal, etc.) variability of directly emitted particles and gas-phase precursors and a complex chemical processing in the atmosphere, elucidation of the chemical composition and physical properties of OA remains challenging. Identification and quantification of OA sources with a sophisticated interpolation of ~~both spatial and temporal variabilities are essential for a development of~~spatial and temporal variabilities are essential for developing effective mitigation strategies for air pollution and a better assessment of the aerosol effect on both health and climate.

OA source apportionment (SA) and PM composition ~~has~~ have been studied extensively using the Aerodyne aerosol mass spectrometer (AMS) (Canagaratna et al., 2007). However, due to the complexity of the AMS measurements and their high operational expenses, AMS campaigns are often limited to short ~~time~~ periods of a few weeks to months. The aerosol chemical speciation monitor (ACSM) allows for unattended long-term observation (>1 year) of non-refractory aerosol particles (Ng et al., 2011a; Fröhlich et al., 2013). It ~~makes it possible to investigate also~~also makes it possible to investigate the long-term temporal variations of OA

sources, which is crucial for policymakers to introduce or validate aerosol-related environmental policies.

Positive matrix factori~~z~~sation (PMF, see Section 3.1 in the Supplement) has been used in various studies for SA of OA (Lanz et al., 2007; Aiken et al., 2009; Hildebrandt et al., 2011; Zhang et al., 2011;~~Lanz et al., 2007;~~ Mohr et al., 2012; Schurman et al., 2015~~; Zhang et al., 2011~~). The multilinear engine (ME-2) implementation of PMF (Paatero, 1999) improves model performance by allowing the use of *a priori* information (constraints on source profiles and/or time series) to direct the model towards environmentally meaningful solutions (Canonaco et al., 2013; Crippa et al., 2014; Fröhlich et al., 2015; Lanz et al., 2008; Ripoll et al., 2015). For long-term data (one year or more) with high time resolution, the composition of a given source could change considerably due to the meteorological and seasonal variabilities. However, a major limitation of PMF is the assumption of static factor profiles, such that it fails to respond to these temporal changes. Therefore, long-term chemically speciated data have been evaluated monthly or seasonally (Petit et al., 2014; ~~Bressi et al., 2016;~~ Canonaco et al., 2015; Minguillón et al., 2015; ~~Petit et al., 2014;~~ Ripoll et al., 2015; Bressi et al., 2016; Reyes-Villegas et al., 2016~~; Ripoll et al., 2015~~) to at least take the seasonal variations into account. To improve the analysis of long-term ACSM datasets, a novel approach that ~~utilizes~~ utilises PMF analysis on a ~~smaller~~ shorter time rolling window was first proposed by Parworth et al. (2015) and further refined using ME-2 by Canonaco et al. (2021)~~Canonaco et al. (2020)~~. The short length of the rolling PMF window allows the PMF model to take the temporal variations of the source profiles into account (e.g., biogenic versus domestic burning influences on oxygenated organic aerosol (OOA)), which normally provides ~~a~~ better separation between OA factors. In addition, using this technique together with bootstrap resampling and a random *a*-value approach allows users to assess the statistical and rotational uncertainties of the PMF results (Canonaco et al., 2021; Tobler et al., 2020).

In this work, we conducted a ~~one~~ one-year ACSM measurement from September 2013 to October 2014 in Magadino, located in an alpine valley in southern Switzerland. We present a comprehensive analysis of the ACSM dataset measured in Magadino using a novel PMF technique, the "rolling PMF". In addition, we also compare the results of the rolling PMF with the source apportionment of offline AMS filter samples (Vlachou et al., 2018) and conventional seasonal PMF analysis.

2 Methodology

2.1 Sampling site

Magadino is in a Swiss alpine valley (46°90'37'' N, 85°60'2'' E, 204 m.a.s.l.), where the sampling site located. This site belongs to the Swiss National Air Pollution Monitoring Network (NABEL, https://www.empa.ch/web/s503/nabel). It is around 1.4 km away from the local train station, Cadenazzo, around 7 km away from the Locarno Airport, and nearly 8 km away from the Lake Maggiore. This station is surrounded by agricultural fields within a rural area, ~~which~~ and is considered as a rural background site. It can be potentially affected by domestic wood burning, adjacent agricultural activity and transit traffic through the valley. The site topography favours quite high PM levels due to stagnant meteorological conditions or boundary layer inversions, especially in winter. The annual average PM_{10} concentration in Magadino exceeded the annual average PM_{10} limit value for Switzerland (20 $\mu g \cdot m^{-3}$) for five years out of the period 2007–2016 (Meteotest, 2017; The Swiss Federal Council, 2018).

2.2 ACSM measurements

In this study, chemical composition and mass loadings of non-refractory constituents of ambient submicron aerosol particles (NR-PM_1) were measured by an Aerodyne quadrupole ACSM (Ng et al., 2011a). The ACSM uses the same sampling and detection technology as the AMS but is simplified and designated for long-term monitoring applications by reducing

maintenance frequency~~,~~ at the cost of lower sensitivity, restriction to integer mass resolution, and no size measurement. Same as for the AMS, sampled submicron particles enter the instrument through a critical orifice (100 µm I.D.) at a flow rate of 1.4 cm^3 s^{-1} (at 20 °C and 1 atm). The sampling flow will pass either through a particle filter or directly into the system using an automated 3-way switching valve~~,~~ that is switched every ~30 s. ~~The sampled particles are focused by an aerodynamic len~~An aerodynamic lens focuses the sampled particles into a narrow beam ~~and~~ which impact on a tungsten surface of around 600 °C, where the non-refractory particles ~~vaporize~~ vaporise and are subsequently ~~ionized~~ ionised by an electron impact source (70 eV). The resulting ions are detected by a quadrupole mass-spectrometer up to a ~~mass to charge ratio~~ mass-to-charge ratio (*m/z*) ~~=~~ of 148 Th. The particle mass spectrum is represented by the difference ~~of~~ between the total ambient air signal and the particle-free signal.

The quantification of ACSM data requires an estimation of the fraction of NR-PM_1 that bounces off the oven without being ~~vaporized~~ vaporised and therefore is not detected (Canagaratna et al., 2007; Matthew et al., 2008). In this study, a constant collection efficiency (CE) factor of 0.45 was applied to take it into account. The details of determinations of CE value was described in Section 1 in the Supplement. ~~A collection efficiency (CE) factor is typically introduced to correct for particle bounce, which depends on the particulate water content (Matthew et al., 2008), ammonium nitrate mass fraction (ANMF) and acidity (Middlebrook et al., 2012). To eliminate humidity effects on CE, a Nafion membrane dryer (Perma Pure MD) was installed on the sampling inlet. In this study, we compared both, a constant CE of 0.45 and a time-dependent CE correction suggested by Middlebrook et al., (2012). It showed that data corrected with a constant CE had a better correlation and slope closer to 1 when comparing with the chromatographic SO_4^{2-}, NO_3^-, and Cl^- anions (Fig. S1a). In addition, as more than 93.5% data have an ANMF smaller than 0.4, only 6.5% of data would be impacted by a time-dependent CE correction, therefore, the ammonium nitrate particles~~

~~doesn't have significant effects on CE for this dataset. Overall, this dataset agrees with external TEOM measurement of both $PM_{2.5}$ and PM_{10} daily mass concentrations as shown in Fig S1c with a constant CE value.~~

In this study, we recorded the data with a time resolution of 30 minutes. During the campaign, ~~T~~the ACSM filament burnt out on 14 ~~April,~~April 2014. This was addressed by switching to the backup filament ~~already~~ installed within the instrument (no venting required). Calibration of the relative ~~ionization~~ ionisation efficiencies (RIE) of particulate nitrate, sulphate, and ammonium ~~was~~ were conducted using size-selected (300 nm) pure NH_4NO_3 and pure $(NH_4)_2SO_4$ particles. Calibrations of the ~~relative ionisation efficiency (~~RIE~~)~~, *m/z* scale, and the sampling flow ~~was~~ were performed every 2 months. In this study, we used the averaged RIEs for nitrate, sulphate, and ammonium, the exact values are shown in **Fig S1** of the Supplement.

2.3 Complementary measurements

Meteorological data, including temperature, precipitation, wind speed, wind direction, and solar radiation are monitored at the NABEL station. In addition, concentrations of trace gases (SO_2, O_3, NO_x), equivalent black carbon (eBC), and PM_{10} were measured with a time resolution of 10 minutes. We used an aethalometer (AE 31 model by Magee Scientific Inc.) to measure eBC concentrations. Therefore, we conducted SA of eBC by following Zotter et al. (2017) using Ångstrom exponents for eBC from traffic $\alpha_{tr} = 0.9$ and wood burning $\alpha_{wb} = 1.68$. More details about eBC source apportionment are provided in Section ~~1~~ 2 of the ~~SI~~Supplement.

2.4 Preparation of the data and error matrices for PMF

In this study, we used acsm_local_1610 software (Aerodyne Research Inc.) to prepare the PMF input matrix. In total, this dataset includes 19'708 time points and 67 ions. Of these, CO_2^+-related variables (I_{O+} (*m*/*z* = 16), I_{HO+} (*m*/*z* = 17), and I_{H2O+} (*m*/*z* = 18)) were excluded from the spectral matrix prior to a PMF analysis. They are reinserted into the OA factor mass spectra

after the PMF analysis using the ratio from the fragmentation table (Allan et al., 2004); the factor concentrations are likewise adjusted. ~~The measurement error matrix was calculated according to Allan et al. (2003, 2004),~~According to Allan et al. (2003, 2004), the measurement error matrix was calculated with a minimum error considered for the uncertainty of all variables in the data matrix as in Ulbrich et al. (2009). Following the recommendations in Paatero and Hopke (2003) and Ulbrich et al. (2009), the measurement uncertainty for variables (*m*/*z*) with a signal-to-noise ratio (S/N) < 2 (weak variables) and S/N < 0.2 (bad variables) were increased by a factor of 2 and 10, respectively. In total, 27 weak ACSM variables were down-weighted. Additionally, *m*/*z* 12 and 13 were not considered during the PMF analyses~~,~~ due to being noisy and their overall negative signal. Moreover, *m*/*z* 15 ~~is~~ was not only very noisy (S/N = 0.09)~~,~~ but may ~~be~~ also affected by high biases due to potential interference with air signals.

~~2.5 Factor analysis of the organic mass spectra~~

~~PMF has been demonstrated to be a useful tool to retrieve the sources of measured organic aerosol mass spectra with a bilinear factor model (Paatero and Tapper, 1994; Ulbrich et al., 2009):~~

$$x_{ij} = \sum_{k=1}^{p} g_{ik} \times f_{kj} + e_{ij} \quad (1)$$

~~where x_{ij} is the mass concentration of the j^{th} mass spectral variable in the time point i^{th}; g_{ik} is the contribution of the k^{th} factor in the i^{th} time point; f_{kj} is the concentration of the j^{th} mass spectral variable in the k^{th} factor; and e_{ij} is the residual of j^{th} variable of the mass spectra in i^{th} time point. The superscript, p represents the number of factors, which is~~

determined by the user. The cost function of PMF uses least squares algorithm by iteratively minimizing the following quantity Q:

$$Q = \sum_{i=1}^{n}\sum_{j=1}^{m}\left(\frac{e_{ij}}{\sigma_{ij}}\right)^2 \quad (2)$$

where σ_{ij} is an element in the $n \times m$ matrix of the measurement uncertainties, which corresponds point-by-point to x_{ij}. In addition, we normalized quantity $\frac{Q}{Q_{exp}}$ as a mathematical metric during PMF analysis, where the Q_{exp} is:

$$Q_{exp} = (n \times m) - p \times (n + m) \quad (3)$$

The $\frac{Q}{Q_{exp}}$ supports the user to determine the number of factors required for the model by investigating the effects on this quantity of adding/removing a factor. However, PMF itself suffers from rotational ambiguity because of the fact that the object function, Q does not provide unique solutions, that is when $\mathbf{G} \cdot \mathbf{F} = \mathbf{G} \cdot \mathbf{T} \cdot \mathbf{T^{-1}} \cdot \mathbf{F}$, PMF provides a similar value of Q but very different solutions (rotated matrix $\bar{\mathbf{G}} = \mathbf{G} \cdot \mathbf{T}$ (rotated factor time series) and $\bar{\mathbf{F}} = \mathbf{T^{-1}} \cdot \mathbf{F}$ (rotated factor profiles)). Only one of or even none of these rotated solutions may be atmospherically relevant. The ME-2 solver (Paatero, 1999) enables theoretically full rotational control over the factor solutions, which is implanted here by imposing constraints via the *a*-value approach on one or more elements of **F** and/or **G** (Paatero and Hopke, 2009). The *a*-value (ranging from 0 to 1) determines how much the resulting factor ($f_{j,solution}$) or time series

~~($g_{j,solution}$) can vary from the input reference factor ($f_{j,reference}$) or time series ($g_{j,reference}$) as shown in Eq. 4a and 4b:~~

$$f_{j,solution} = f_{j,reference} \pm a \cdot f_{j,reference} \quad (4a)$$

$$g_{j,solution} = g_{j,reference} \pm a \cdot g_{j,reference} \quad (4b)$$

~~Previous work using *a*-values has shown to efficiently retrieve environmentally reasonable PMF solutions. This is due to the presence of legitimate *a priori* constraints which decrease the degree of rotational ambiguity (Canonaco et al., 2013, 2020; Crippa et al., 2014; Lanz et al., 2008). Here we configured the ME-2 solver and analysed PMF results using SoFi (Source Finder, Datalystica Ltd., Villigen, Switzerland) Pro 6.D interface (Canonaco et al., 2013, 2020), developed within the IGOR Pro software (WaveMetrics Inc., Lake Oswego, OR, USA).~~

2.5 Rolling PMF analysis with ME-2

In this study, we conducted a series of steps (~~section~~Section 3.2 and 3.3 in ~~SI~~the Supplement) to obtain the results we presented in this manuscript. In summary, we first tested potential sources for each season with seasonal PMF *pre-tests*, secondly, we obtained stable seasonal solutions from bootstrap seasonal analysis. Then, we conducted rolling PMF with certain settings (constraints, number of repeats, length of the window size, and step of rolling window). Lastly, we were able to retrieve robust results using specific criteria to define environmental reasonable solutions. Please refer to ~~section~~Section 3.2 and 3.3 ~~of SI~~in the Supplement for more detailed description of each step. In this section, we focus on the general introduction of rolling PMF with ME-2, the differences between our method vs. the method developed by Canonaco et al. (2021), and the general settings of the rolling PMF analysis in this study.

Running PMF over the long-term ACSM datasets assumes that the OA source profiles are static within this time window. ~~This~~ It can lead to large errors~~,~~ since OA chemical fingerprints are expected to vary over time (Paatero et al., 2014). For example, Canonaco et al. (2015) showed that the variability of summer and winter OOA cannot be accurately represented by a single pair of OOA profiles. A common way to reduce the model uncertainty arising from this source is to choose a proper number of OA factors (Sug Park et al., 2000)~~,~~ and then perform a PMF analysis on a subset of measurements to capture temporal features of OA chemical fingerprints. Such ~~characterization~~ characterisation of OA sources on a seasonal basis has been demonstrated in a number of studies (-Lanz et al., 2008; Crippa et al., 2014; Petit et al., 2014; ~~Lanz et al., 2008;~~ Minguillón et al., 2015; ~~Petit et al., 2014;~~ Ripoll et al., 2015; Zhang et al., 2019). ~~(~~Parworth et al.~~,~~ (2015) introduced the rolling PMF by running PMF on a small window (14 days), which advanced with a step of 1 day. This novel technique enables the source profiles to adapt to the temporal variabilities. Canonaco et al. (2021) combined the rolling PMF technique with ME-2 (Section 3.1 in the Supplement) to deal with the rotational ambiguity of the PMF analysis. In addition, it also used the bootstrap resampling strategy (Efron, 1979) and random *a*-values (Section 3.2.2 in the Supplement) to estimate the statistical and rotational uncertainties of the PMF analysis.

In this study, we mostly followed the methods developed by Canonaco et al. (2021), but with some modifications. The settings of the rolling PMF window is explicitly explained in Section 3.2.3 of the Supplement). In addition, we also performed a test of rolling window size (i.e., 1, 7, 14, and 28 days) using a similar approach (Section 4 in the Supplement). As Canonaco et al. (2021) did, we also used the criteria-based selection function developed by Canonaco et al. (2021) to evaluate our PMF runs. The settings of the criteria are provided in Section 3.2.4 of the Supplement.

However, instead of using published reference factor profiles like Canonaco et al. (2021) have done, we retrieved the reference profiles of primary and local factors from seasonal bootstrap analysis (Section 3.2 in the Supplement). Specifically, the reference profiles of hydrocarbon-like OA (HOA) factor and biomass burning OA (BBOA) factor were retrieved from winter (December, January, and February, DJF) bootstrapped PMF solution as shown in **Fig. S4**, and we got the *m/z* 58 related (58-OA) factor profile from summer (June, July, and August, JJA) bootstrapped PMF solution (**Fig. S4**). The 58-OA was dominated by nitrogen-containing fragments (at *m/z* 58, 84, and 98). In general, ACSM estimates organic *m/z* 98 signal by dividing organic *m/z* 84 to a factor of 2 according to the fragmentation table of organic species that was provided by Allan et al. (2004). Thus, the intensity of *m/z* 98 is always half of the intensity of *m/z* 84 in each factor. This 58-OA only appeared after the filament was switched on 14 April 2014. The instrument setup thus ~~influenced strongly~~strongly influenced the sensitivity of these components ~~(likely~~ due to influences of surface ioni~~z~~sation~~)~~. The nitrogen-containing ion, *m/z* 58, was also observed in ~~(~~Hildebrandt et al.~~,~~ (2011) due to the enhanced surface ionisation in a certain period. In addition, the potassium signal enhanced at the same time, which further corroborated our hypothesis of the enhanced surface ionisation. Also, since this factor was constrained through the whole dataset, the PMF model overestimated the mass concentration of this factor significantly, which leads to high uncertainties for the 58-OA. Therefore, the time series of this source should be considered as the upper limit, and the real mass concentration of it could be substantially lower. However, with the low mass concentration of the 58-OA during the whole campaign, we considered it as a minor factor. Thus, this factor was considered in the PMF analysis, but no further interpretation of its potential source will be attempted in this manuscript~~. Therefore, we believed this factor was still environmental relevant.. H owever, it remains challenging to understand its real source with the limited mass to charge resolution of ACSM. In addition, the contribution of this source~~

~~cannot be quantified consistently since the sensitivities for the key ions in this factor changed in the middle of the campaign. Therefore, this factor was considered in the PMF analysis, but no further interpretation of its potential source will be covered in this manuscript.~~ Moreover, we took a different path to define "good" PMF solutions by using a novel student *t*-test approach to determine the environmentally reasonable solutions quantitatively with minimum subjective judgements (Section 3.3 in the Supplement). Overall, we provided a comprehensive analysis of a long-term ACSM dataset using this state-of-the-art technique in this work. The results were unfolded in the following section.

~~Rolling PMF analysis with ME-2~~

~~In this study, we performed PMF runs with *a priori* constraints (factor profiles) retrieved from seasonal bootstrap analysis (Section 2.2 in the SI) on a small and rolling window (i.e., 1, 7, 14, and 28 days) that could move across the entire dataset with a step of one day (Canonaco et al., 2020; Parworth et al., 2015). In addition, we used the bootstrap re-sampling strategy, which can randomly choose a subset of the original matrix and replicate some of the rows/columns to create a new same-size matrix (Efron, 1979). Here, we combined this rolling PMF analysis with the bootstrap strategy and random *a*-values for constrained factor profiles to estimate the statistical and rotational uncertainties of this PMF analysis. More details of this novel technique is found in Canonaco et al. (2020).~~

~~2.5.1 Window settings~~

~~In order to retrieve appropriate constraints, we performed PMF *pre-tests* and bootstrap analysis for different seasons. More details of the steps, settings of these analysis can be found in Section 2 of the SI. Here, we constrained primary OA factor profiles (hydrocarbon-like OA factor (HOA) and biomass burning OA (BBOA)) as well as the factor profile of a local factor (LOA)~~

using the *a*-value technique in the rolling PMF analysis. The reference profiles of HOA and BBOA were from the winter bootstrapped PMF solution (Dec, Jan, and Feb) as shown in Fig. S6. With a higher contribution of the biomass burning trace ion *m/z* 60 in the winter, we expect a more representative and robust BBOA profile from the winter solution than from other seasons. The LOA profile was retrieved from the summer bootstrapped PMF solution (Jun, Jul, and Aug) (Fig. S6). To allow the factor profile to adapt itself over time, a random *a*-value within a range of 0.4 with a step of 0.1 is applied for HOA and BBOA. Canonaco et al. (2020) suggested that an upper *a*-value of 0.4 is sufficient to cover the temporal variation of OA source profiles. Moreover, due to the uniqueness of the LOA chemical profile, it is tightly constrained with a constant *a*-value of 0.05. The LOA factor appeared only after the filament had been changed (14 April, 2014), and its mass spectrum is dominated by nitrogen-containing fragments (at *m/z* 58, 84, and 98).

In total, we constrained HOA and BBOA factors with random *a*-value (0–0.4, with a step of 0.1), and an exact *a*-value (0.05) for LOA factor in the rolling PMF analysis. There are 25 (N=5×5) possible *a*-value combinations within an individual rolling window. Therefore, 50 PMF iterations for each time window are sufficient to cover all possibilities of the *a*-value combinations. With the rolling window of 50 repeats, each data point (except the data within the first and last time window) will actually have many PMF iterations (i.e., N=length of the window×50), where bootstrap resampling and random combinations of constraints is performed. This allows to estimate the statistical and rotational uncertainties of the PMF factors (Canonaco et al., 2020). To find the optimum length of the time windows, we tested four different lengths of the time windows (N=1, 7, 14, 28) using the same approaches as in Canonaco et al. (2020). We determined the optimum length of the time window based on the number of missing data points (un-modelled data due to the selection based on the criteria) while applying the same thresholds for the same criteria.

2.5.2 Criteria settings

Performing a rolling analysis for a one-year data with 50 repeats per window requires several tens of thousands of PMF runs. Manual inspection of all PMF runs is impractical and therefore was replaced by monitoring user-defined criterion scores (Canonaco et al., 2020). In this study, R^2 values of the time series of modelled HOA vs NO_x and eBC_{tr} were used for HOA. The BBOA factor was inspected using the variation of *m/z*=60 explained by BBOA (Table S1). For these time series based criteria, (criterion 1 to criterion 3 in Table S1), we deployed student t-test to minimize subjective judgment while determining the thresholds (more discussions in Section 2.3 of the SI).

Typically, OOA factors are dominated by the signals of f_{43} ($C_2H_3O^+$ at *m/z* = 43) and f_{44} (CO_2^+ at *m/z* = 44) that correspond to the less and more oxygenated ion fragments (Canonaco et al., 2015; Ng et al., 2010), where *f* is the fraction of a variable, *i.e.* the intensity $I_{m/z}$ normalized by the sum of the intensities of all organic *m/z* variables. In this study, we were able to retrieve two OOA factors (i.e., more oxidized OOA (MO-OOA) and less oxidized OOA (LO-OOA)) for the whole year, while MO-OOA can be at either at 4th or 5th position because there are two unconstrained factors. Thus, we used the f_{44} for the 4th factor to sort the unconstrained OOA factors to ensure MO-OOA and LO-OOA sitting on the 4th and 5th position, respectively. The details of the sorting scheme can be found in Canonaco et al. (2020). At the same time, we also monitored the f_{43} in LO-OOA and f_{44} in MO-OOA to make sure they are not zero. With this set of criteria, we were able to only select "good" (atmospherically relevant) PMF runs before averaging.

3 Results and discussion

3.1 Overview of PM_1 sources in Magadino

Considering that the major part of eBC is within PM_1 (Schwarz et al., 2013), we added eBC to the total NR-PM_1 from the ACSM to perform a mass closure analysis ~~with~~ using independent measurements of $PM_{2.5}/PM_{10}$ from filters. The gravimetric $PM_{2.5}$ and PM_{10} show a high correlation with the total estimated PM_1 (NR-PM_1 +eBC) (**Fig. S1c**). The slopes of the linear fits (± 1 standard deviation) are 1.62 ± 0.05 (R^2 = 0.81, N=79) for $PM_{2.5}$ *vs.* PM_1 and 1.84 ± 0.03 (R^2 = 0.67, N=335) for PM_{10} *vs.* PM_1. ~~This~~ It means that the estimated PM_1 comprised 62% and 54% of the $PM_{2.5}$ and PM_{10} mass, respectively. The daily averages of ~~the~~ inorganic species concentrations measured by the ACSM and those measured on the filters by ion chromatography showed a ~~high~~ good correlation, with R^2 = 0.83 for SO_4^{2-}, R^2 = 0.82 for NO_3^- and R^2 = 0.50 for Cl^-, with slopes close to 1 (**Fig. S1a**). The 2-week average of total ammonium and total nitrate measured by the offline AMS technique agreed rather well with the ACSM ammonium (R^2 = 0.47) and nitrate (R^2 = 0.79), as shown in the plots in **Fig. S1b**. The ion balance of particulate ammonium, sulphate and nitrate measured by the ACSM showed that the measured aerosol particles were mostly neutral.

The daily average PM_1 components are shown in **Fig. 1**~~**Fig. 1**~~**a**, with ~~the~~ an annual average PM_1 concentration (including eBC) ~~for the period~~ from September 2013 to October 2014 equal to 10.2 µg m^{-3}. In winter, the average PM_1 concentration was highest (13.8 µg·m^{-3}), with OA contributing 54% to the total PM_1 mass. In summer, the average PM_1 mass concentration was below 10 µg·m^{-3}, but the relative contribution of the OA fraction increased to 62%.

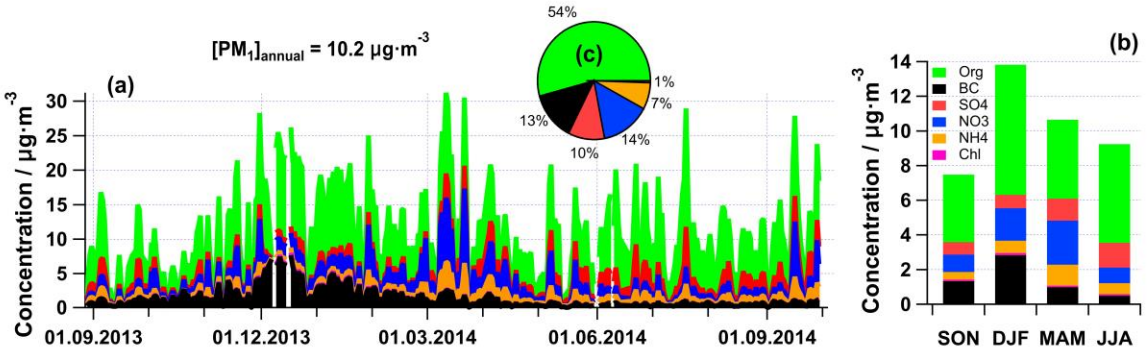

Fig. 1 Chemical composition of PM_1 in Magadino 2013-2014 – daily (a), seasonal (b) and annual (c) averages. The labels indicate ~~the~~ non-refractory organics (Org), sulphate (SO_4), nitrate (NO_3), ammonium (NH_4) and chloride (Cl) ~~ions~~ measured by the ACSM, and ~~the~~ black carbon (BC) measured by light absorption.

Seasonally averaged diurnal cycles of NR-PM_1 components and ~~of~~ eBC are displayed in **Fig. 2**~~Fig. 2~~. In this study, all the data is based on local time (Central European Time). In fall, spring and summer, the diurnals of these pollutants seem to be mainly affected by the development of the boundary layer height (BLH)~~BLH, m~~. Most of the species show similar diurnal trends for these three seasons. In addition, summer has the highest sulphate concentration~~,~~ due to the enhanced photochemical production. In winter, air pollutants are accumulated during the evening and night due to the thermal inversion. In general, eBC and organics have higher levels due to enhanced biomass burning emissions and a lower BLH ~~boundary layer height (BLH)~~. We observed distinct midday peaks of organics, sulphate, nitrate, ammonium, chloride, and NO_x in the winter. Magadino experienced a series of windless, cold, but sunny periods from December 2013 to January 2014, including such sharp peaks (**Fig. S6a**). ~~It~~ This ~~is interpreted to be~~was due to advection within the shallow boundary layer ~~due to the fact that~~as both primary and secondary pollutants increased simultaneously. At the same time, the ~~L~~local wind~~s were very low~~ speed near the ground was very low. ~~but likely~~ One potential explanation was that the locally and regionally induced orography influenced winds, including vertical diffusion

processes, caused these delayed midday peaks. However, these processes remain ~~were initiated during these times that are~~ difficult to track without spatially distributed measurements~~.~~. Such phenomena were not observed during cloudy, cold, and windless days (**Fig. S6b**) without thermally induced meteorological processes. Unlike other seasons, the dilution process due to vertical mixing happened only after noon time due to strong inversions during the night and late irradiation of the valley surface in the winter.

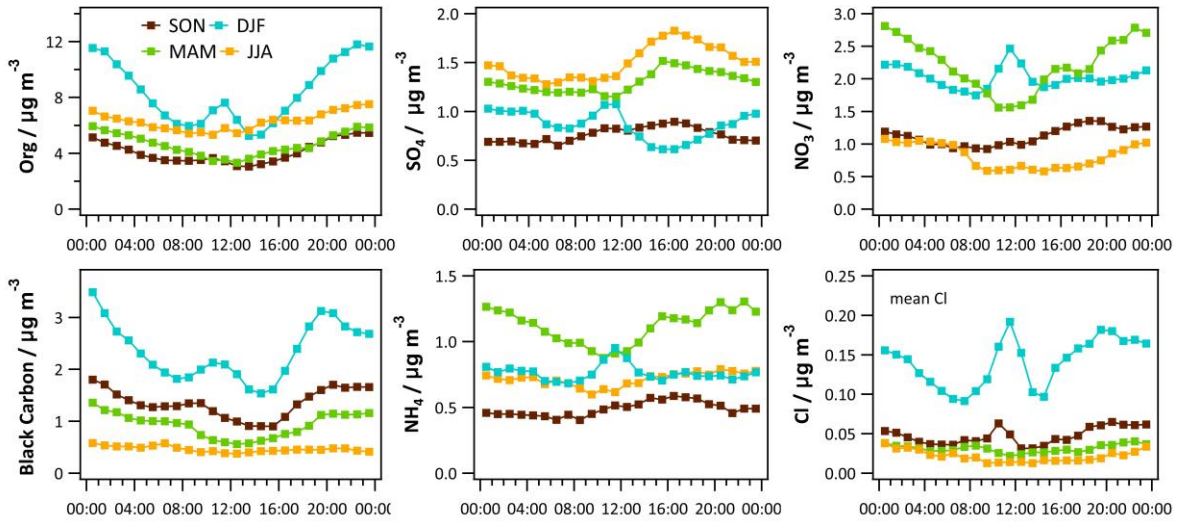

Fig. 2 Seasonal, diurnal cycles of the measured PM_1 components (hourly averages) for the organic and inorganic species (sulphate, nitrate, ammonium, and chloride) of the ACSM, and equivalent black carbon. ~~Seasonal diurnal cycles of PM_1 constituents calculated as an hourly average for ACSM organic and inorganic species (sulphate, nitrate, ammonium, and chloride) and equivalent black carbon.~~

3.2 Seasonal PMF *Pre-tests*

The automated rolling PMF analysis requires the knowledge of the reference profiles as well as the number of factors. ~~In this section, we present~~This section presents how the number of factors ~~were~~ was determined based on seasonal PMF *pre-tests* (refer to Section 3.2.1 in the Supplement for methodology). Initially, unconstrained PMF (3 to 6 factors) was performed separately for the different seasons by following the SA guidelines provided by Crippa et al.

(2014). Typically, the HOA profile is ~~characterized~~ characterised by a high contribution of alkyl fragments (*e.g. m/z* =43, *m/z* =57) and the corresponding alkenyl carbo~~-~~cations (*e.g. m/z* = 41, *m/z* = 55), and the factor profile is relatively consistent over time and different locations. The BBOA profile exhibits significant signals at *m/z* = 60 and *m/z* =73, which are well-known fragments~~,~~ arising from fragmentation of anhydrous sugars present in biomass-related emissions (Alfarra et al., 2007). ~~For the unconstrained PMF runs, the HOA profile is present throughout the whole year~~The HOA profile is present throughout the whole year for the unconstrained PMF runs, while the BBOA profile exists for all seasons except in summer. However, as shown in **Fig. S2**, the measured fraction of *m/z* = 60 during summer was above the background level of 0.3% ±0.06% for biomass burning-related air masses~~, 0.3% ±0.06%~~ (Aiken et al., 2009; Cubison et al., 2011; DeCarlo et al., 2008). In addition, the scaled residual at *m/z* = 60 was decreased when a BBOA factor profile was constrained. Thus, we decided to constrain the BBOA factor for all seasons to potentially capture some local events, such as ~~agricultural and~~some open fires and barbeques in summer.

No evidence for the presence of a cooking-related OA (COA) factor was found based on the seasonal pre-analysis of the key fragments (*m/z* 55 and *m/z* 57). **Figure S3** ~~It~~ shows no difference in the slope of the absolute mass concentration of *m/z* 55 vs *m/z* 57 for different hours of the day (**Fig. S3a**), while different seasons show different slopes (**Fig. S3b**). Therefore, a COA factor was not considered in the PMF model. Moreover, a rapid increase of the measured fraction of *m/z* = 58, 84, and 98 together with *m/z* 39 (potassium signal) was observed after a filament exchange on 14 April, 2014. It ~~is~~ was likely that the ACSM's sensitivity towards those ions was changed by the filament exchange. Also, this ~~LOA~~58-OA factor was present for spring, summer, and autumn in 2014 in unconstrained PMF runs all the time after the filament change. Therefore, we kept this factor for these three seasons.

For the factor(s) with a secondary origin, we performed PMF models with a different number of factors (3–6) ~~were tested~~ to assess if the oxygenated OA (OOA) factor ~~(with a high contribution of *m/z* 44 that is likely dominated by the CO_2^+ ion, derived from decomposition of carboxylic acids (Duplissy et al., 2011))~~ is separable without mixing with primary organic aerosol (POA) factors ~~(Fig. S6)~~(with a high contribution of *m/z* 44 that is likely dominated by the CO_2^+ ion, derived from decomposition of carboxylic acids (Duplissy et al., 2011)). We conducted these tests (with a different number of factors) independently for the different seasons (autumn 2013, winter, spring, summer, autumn 2014).

We analysed the winter data first by constraining an HOA factor profile (Crippa et al., 2013) with a tight *a*-value of 0.05. The 3-factor solution (with one OOA factor, i.e., less oxidized OOA (LO-OOA) and more oxidized OOA (MO-OOA)) showed similarly good agreement of HOA and BBOA with the external tracers (NO_x, eBC from traffic source (eBC_{tr}), eBC from wood burning source (eBC_{wb})) as the 4-factor solution (with two OOA factors). However, the scaled residual of *m/z* 60 was reduced for the solution with two OOA factors. Moreover, the solution with one OOA factor was not sufficient to explain the variabilities of measured f_{44} vs f_{43} (excluding the primary organic aerosol (POA) factors). For 5- and 6-factor solutions, the BBOA and LO-OOA factors started to split. Eventually, we selected the 4-factor solution (HOA, BBOA, MO-OOA, LO-OOA) as the best representation of the winter data.

After the bootstrap seasonal PMF runs of the winter data (details in Section ~~2~~ 3.2.2 of the ~~SI~~Supplement), we extracted the HOA and BBOA profiles to use them as the reference factor profiles (**Fig. S4**) for the *pre-tests* of other seasons. For the spring, summer, and autumn seasons, 3- to 6-factor PMF solutions were modelled separately for each season by constraining the HOA (*a*-value=0.1) and BBOA (*a*-value=0.3) profiles. For the 3-factor solution, we observed an OOA factor with some signals at *m/z* 58, 84, and 98 which we could not relate to a specific

source or process. Also, the scaled residuals of variables showed significant levels for these three ions. In addition, the time series and factor profile of 58-OA were so distinct that PMF could easily resolve it. When we increased the number of OA factors from 3 to 4, a factor dominated by *m/z* 58, 84, and 98 emerged, ~~which we~~ named ~~local organic aerosol (LOA~~58-OA~~)~~. However, the OOA factor still showed slight signals at *m/z* 58, 84, and 98. An increase in the number of factors from 4 to 5 did not only result in a decrease in $\frac{Q}{Q_{exp}}$, but also in "clean" OOA factors without mixing with the ~~LOA~~58-OA factor. A further increase in the number of factors did not change $\frac{Q}{Q_{exp}}$ substantially (< 1%), and the sixth factor was a mathematical split of the ~~LOA~~58-OA factor with *m/z* 58 as the dominating variable. Thus, the 5-factor PMF model was chosen as the most appropriate for the spring, summer, and autumn 2014 to be able to isolate this instrumental artifact via PMF. Note that we did not add the ~~LOA~~58-OA factor for the autumn season in 2013 since it appeared only after the filament exchange on 14 April, 2014. This ~~LOA~~58-OA factor was included while running PMF because of the rapid drop of the $\frac{Q}{Q_{exp}}$ from 4 to 5 factors in the PMF model, but the source of this factor will not be discussed in the manuscript.

3.3 Full-~~-~~year rolling PMF analysis

Here we present the ~~optimized~~ optimised time window size (14 days) (details of the time window ~~optimization~~ optimisation are given in Section 4 of the ~~SI~~Supplement and in **Fig S10**). In total, we considered 53.4% of the PMF runs (11087 out of 20750) with only 11 non-modelled data points. The results of the full-year PMF analysis of the 30-min resolved ACSM data are ~~summarized~~ summarised in **Fig. 3~~Fig. 3~~**. The relative contributions of the OA factors are in addition shown in **Fig. 3~~Fig. 3~~b**. The primary ~~traffic~~ traffic-related HOA had very little variation (seasonal averages between 8.1 and 10.1%) throughout the year (**Fig. 4~~Fig. 4~~**). In contrast, BBOA showed a distinct yearly cycle (8.3–27.4%) with a yearly averaged

contribution of 17.1%. It increased significantly (to 27.4%) in winter which is typical for Alpine valleys (Szidat et al., 2007). It means that biomass burning was the most important primary OA source during the cold season in Magadino. The eBC_{wb} showed similar trends as the BBOA factor time series during the cold seasons (**Fig. 3~~Fig. 3~~c**). The contribution of ~~LOA~~58-OA remained small before the filament was changed on 14 April~~,~~ 2014, which is expected because we could not retrieve this factor in seasonal unconstrained PMF runs before April 2014.

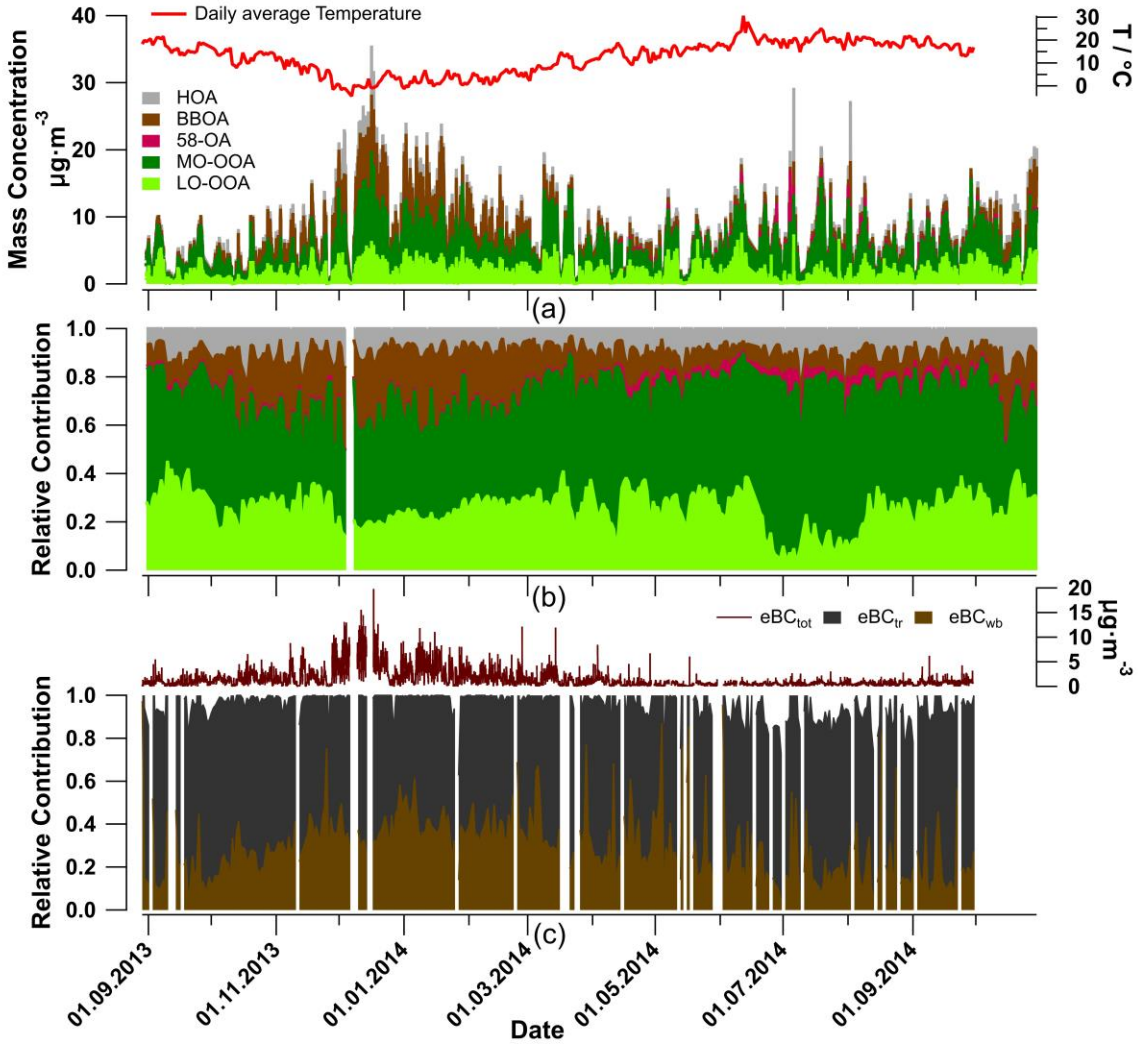

Fig. 3 Annual cycles of OA ~~sources~~components: (a) absolute and (b) relative OA contributions plotted as 30-min resolved time series, (c) BC source apportionment.

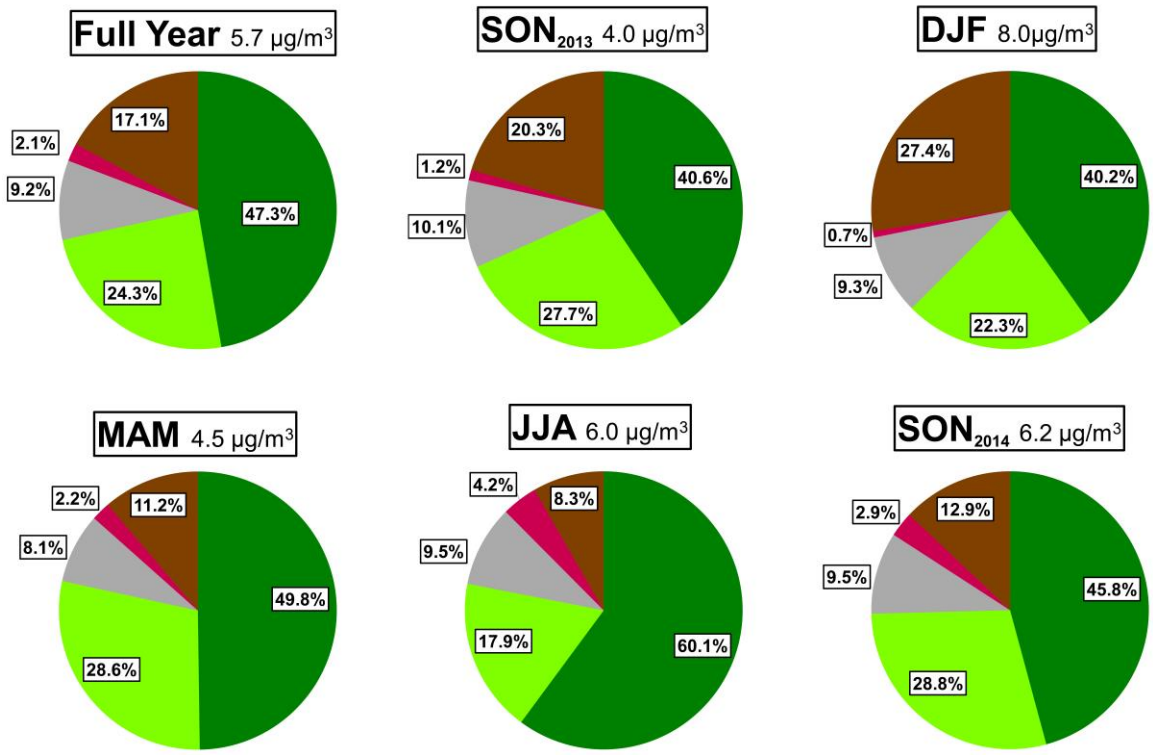

Fig. 4 OA pie charts for the whole year and ~~for~~for the ~~-~~different seasons.

In this study, we retrieved two OOA factors, LO-OOA and MO-OOA. Total OOA (LO-OOA+MO-OOA) contributed substantially to the total OA mass throughout the whole year, with an average contribution of 71.6% (Fig. 3~~Fig. 3~~**b**; Fig. 4~~Fig. 4~~). In general, the contribution of OOA to the total OA mass did not vary distinctly over the seasons~~,~~ but reached a maximum of 90.1% on 12 June~~,~~ 2014, the day with the highest daily average temperature (30.7 °C).

In this work, we ~~did~~ made head-to-head comparisons between the ~~bootstrap seasonal~~seasonal bootstrap solutions and the rolling PMF results (see Fig. A1~~Fig. A1~~, Fig. A2~~Fig. A2~~, Fig. A3~~Fig. A3~~, and Table A1~~Table A1~~ in the Appendix) in terms of mass concentrations, factor profiles, scaled residuals, and correlations between time series for each factor and corresponding external tracers. We found consistent factor profiles and mass concentrations

for the constrained factors (i.e., HOA, BBOA, and ~~LOA~~58-OA), while OOA factors showed quite some differences in both mass concentrations and factor profiles. Rolling PMF provided slightly better correlations and smaller scaled residuals~~, t~~. Therefore, we consider rolling PMF results to be more environmentally reasonable than those of the seasonal PMF (more details in Appendix A).

3.3.1 ~~Optimized~~ Optimised OA factors retrieved from a rolling PMF model

The primary and secondary OA factors retrieved as an annual mean of all ~~optimized~~ optimised PMF solutions together with their diurnal cycles for all seasons are shown in **Fig. 5~~Fig. 5~~**. ~~Seasonal variations of the OOA factor profiles are demonstrated in Fig. 7 and further discussed in more detail in Section 3.3.2.~~ Note that the primary factors (HOA, BBOA, and ~~LOA~~58-OA) were constrained, where the ~~LOA~~58-OA profile was tightly constrained with an *a*-value of 0.05 due to the uniqueness of its chemical profile~~. Therefore, only a small variation was allowed for LOA~~, while the HOA and BBOA model profiles varied more due to looser constraints (**Fig. S8**). HOA and BBOA ~~have~~ had averaged *a*-values of 0.207±0.036~~,~~ and 0.195±0.050, respectively. In addition, they both ~~had~~ showed good agreement with previous studies (Crippa et al., 2014; Ng et al., 2011b). The probability distribution function (PDF) of applied *a*-values for selected PMF runs ~~over~~ vs time was also investigated (**Fig. S8**). Most selected runs chose *a*-values of 0.1–0.3 for HOA and BBOA. The OOA factors show larger variations in the chemical profiles because these two factors were not constrained due to the high variability of oxidation processes governing the secondary factors.

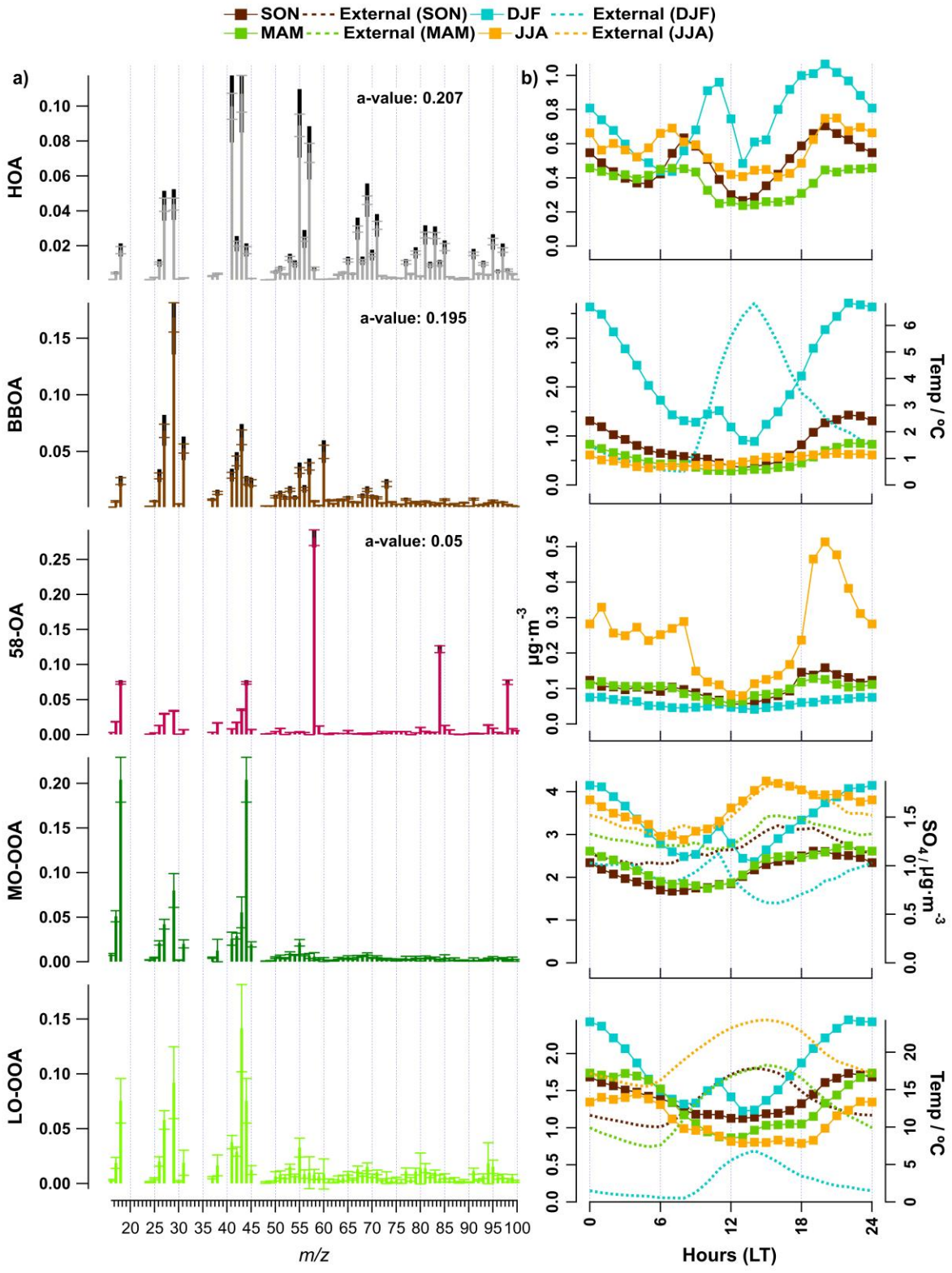

Fig. 5 Overview of the primary and secondary OA components ~~sources~~ in Magadino in 2013-2014: (a) OA factor profiles and (b) seasonal diurnal cycles of HOA, BBOA, LOA, MO-OOA, and LO-OOA. The ambient temperature is shown on the LO-OOA diurnal plots~~, respectively~~. In (a) the error bar is the standard deviation; the black bars show the maximum and the minimum that the variable was allowed to ~~be~~ vary from the reference profiles. The average, 10th, and 90th percentiles for a-values of HOA are 0.195, 0.007 and 0.378, respectively. Also,

the average, 10th, and 90th percentiles for a-values of BBOA are 0.202, 0.025 and 0.379, respectively.

Due to extensive residential wood combustion combined with winter inversions, the concentrations of BBOA and eBC_{wb} were three times higher at night than at midday. As discussed above, during winter, all of the air pollutants, including all PMF factors peaked concurrently at 10–11 a.m. (local time) due to ~~development~~ delayed illumination of the valley site and slow wind speed near the ground~~of the mixed boundary layer~~ (light blue markers in **Fig. 2**~~**Fig. 2**~~ for total PM_1 and **Fig. 5**~~**Fig. 5**~~**b**). In summer, an additional local photochemical production led to an increasing MO-OOA mass during the day (red markers in **Fig. 5**~~**Fig. 5**~~**b**), similar~~ly to the diurnal behaviour of sulphate~~ to the sulphate diurnal behaviour (R^2=0.63). A night~~-~~time increase and a daytime decrease of the LO-OOA mass during spring and summer apparently followed condensation and re-evaporation cycles of semi-volatile species, similar to the behaviour of ammonium nitrate. Additionally, nocturnal chemistry of NO_3/N_2O_5 radicals could lead to the formation of HNO_3 *via* N_2O_5 hydrolysis and of organic nitrates *via* oxidation of VOCs (Brown et al., 2004; Dentener and Crutzen, 1993), thus influencing the diurnal cycles of both particulate nitrate and LO-OOA (with R^2 = 0.48 for spring and R^2 = 0.36 for summer).

~~In **Fig. 6**~~~~**Fig. 6**~~~~, we also present~~ also presents the diurnal cycles of HOA, eBC_{tr} and NO_x with different patterns for weekdays and weekends. The hourly averages of HOA and eBC_{tr} a~~s well as~~nd the NO_x mixing ratio peak during the morning and evening rush hours over the weekdays, while on the weekends there is only an evening pollution increase coinciding with the time when people come back from holidays or night~~-~~time leisure activities.

Formatte

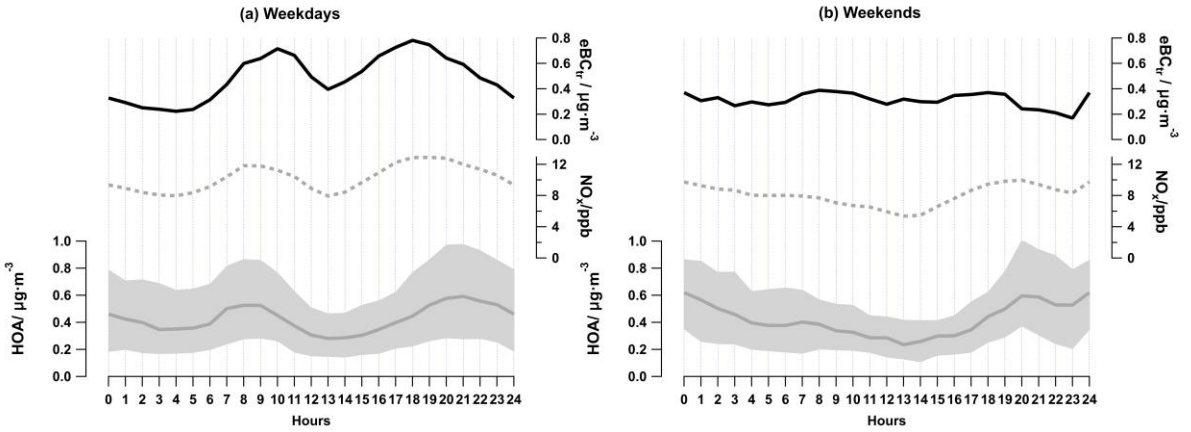

Fig. 6 Diurnal cycles of HOA (grey symbols), black carbon apportioned to traffic emissions eBC_{tr} (dashed lines) and NO_x (dotted lines) for weekdays (a) and weekends (b). The shaded areas represent the interquartile range for HOA (1-hour averages) ~~HOA~~.

3.3.2 f_{44}/f_{43} analysis of secondary OA factors

While *m/z* 44 is mostly from the fragment of CO_2^+, a fingerprint of oxygenated species, *m/z* 43 can originate from $C_2H_3O^+$ (a fingerprint of semi-volatile species) or $C_3H_7^+$ (a fingerprint of the primary emissions of hydrocarbon-like species) (Canonaco et al., 2015; Chirico et al., 2010; Ng et al., 2010). Thus, f_{44} and f_{43} are often used to identify the oxidation state of the factors, which is ~~important~~ crucial to differentiate the MO-OOA and LO-OOA factors. Under the premise that the POA factors and the ~~LOA~~58-OA factor are all well-resolved, it is ~~important~~ essential to investigate the relationship between the *m/z* 44 and *m/z* 43 signals in the OOA factors to determine whether or not one/two OOA factors are sufficient to explain the dataset. In addition, the shapes of the ~~clouds~~ yellow-red dots shown in an f_{44} vs f_{43} plot (**Fig. 7**~~**Fig. 7**~~) may also include some source-related information. **Fig. 7**~~**Figure 7**~~ depicts the relationship between f_{44} and f_{43} of ~~the~~ two modelled OOA factors for the different seasons. The yellow cloud of data points represents the measured f_{44} vs f_{43} after subtracting the *m/z* 44 and *m/z* 43 signals contributed by the primary HOA, BBOA and ~~LOA~~58-OA factors (Eq. S11 and Eq. S12). They are colour coded by the total OA mass concentration (data points with OA mass concentration below 2 µg·m^{-3} are hidden).

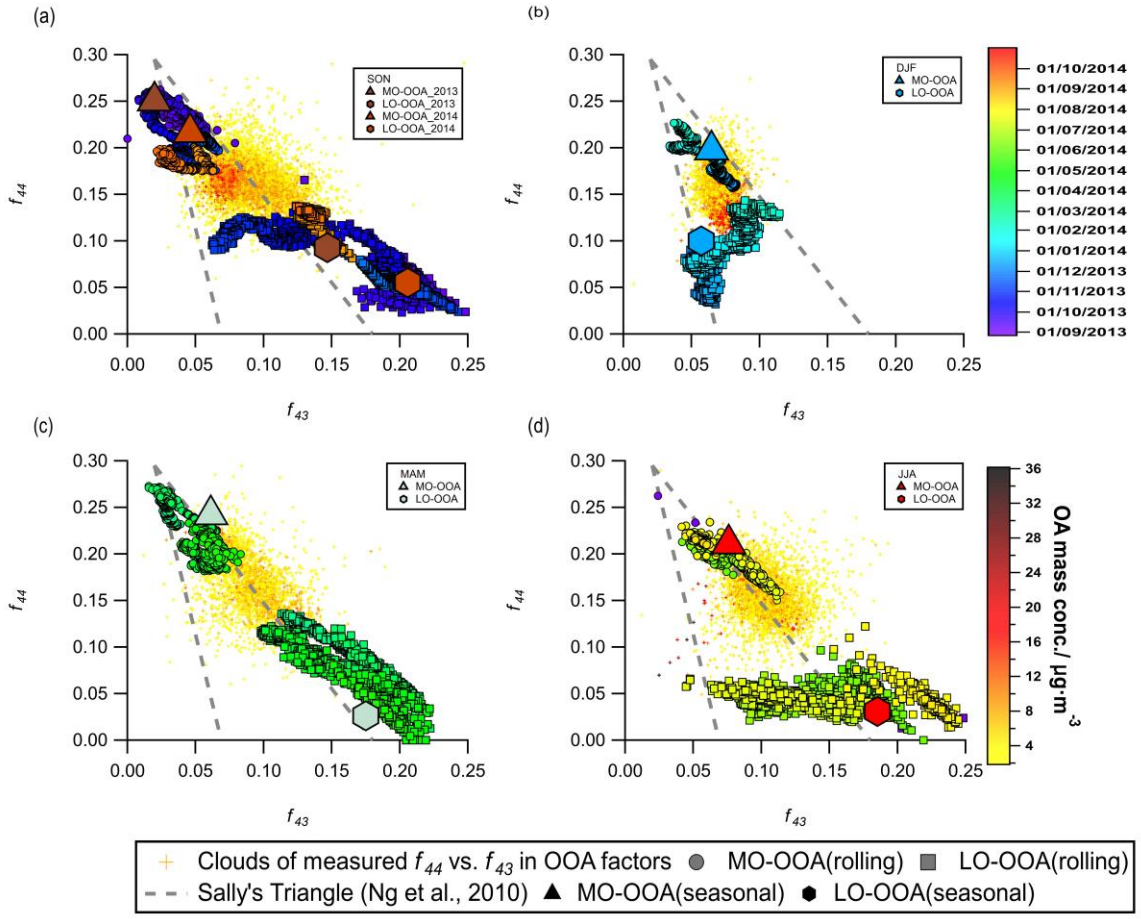

615

616 **Fig. 7** ~~OOA~~ f_{44} and f_{43} of OOA (after subtraction of signals contributed by the primary HOA,
617 BBOA and 58-OA factors) for four different seasons. The small yellow/red ~~cloud~~ crosses of
618 data points represent~~s~~ the f_{44} vs f_{43} ~~by subtracting the f44 and f43 contributed from HOA, BBOA~~
619 ~~and 58 OA factors~~. They are colour-coded by the total OA mass concentration. The bigger size
620 of ~~circles, triangles, and squares~~hexagons represent the ratios between f_{44} and f_{43} intensities
621 within the factor profiles of MO-OOA and LO-OOA in seasonal solutions, respectively. ~~While~~
622 ~~t~~The smaller size of circles ~~, triangles,~~ and squares are ratios between f_{44} and f_{43} intensities
623 within the factor profiles of MO-OOA and LO-OOA from rolling PMF analysis, which are
624 colour-coded by ~~the~~ date and time. The dashed lines represent~~are the~~ Sally's triangle from ~~(~~Ng
625 et al., (2010)~~(Ng et al., (2011b)~~ and depict~~s~~ the region where OOA from ~~several~~ multiple PMF
626 ~~OOA~~analyses ~~from~~during the last decade resided in the f_{44} vs f_{43}~~f44 vs f43~~ space.

627

628 As shown in **Fig. 7**~~**Fig. 7a**~~, the data points in Sep–Oct (both in 2013 and 2014) were located
629 on the right side of the triangle presented first by Ng et al. (2010), while the November (2013)
630 data points were located within the triangle. In addition, the spring and summer data points
631 (**Fig. 7**~~**Fig. 7c**~~ and **Fig. 7**~~**Fig. 7d**~~) were all located rather on the right side of the triangle, but
632 the winter points lied within the triangle (**Fig. 7**~~**Fig. 7b**~~). We made a similar plot but with

monthly resolution and different colour codes in **Fig. S9.** The data points located within the triangle correspond to the time with a lower temperature than those that are closer to the right side of the triangle ~~(~~in **Fig. S9**~~)~~. It ~~This~~ could be explained by the increased biogenic OOA ~~emissions~~ contributions when the temperature was higher, as biogenic OOA tends to be distributed along the right side of the triangle (Canonaco et al., 2015; Pfaffenberger et al., 2013). Also, when the temperature decreases, the increased biomass emissions make the OOA points ~~to~~ lie vertically within the triangle (Canonaco et al., 2015; Heringa et al., 2011), which is the case for the winter data (**Fig. 7**~~**Fig. 7**~~**b**).

In July 2014, the rolling PMF LO-OOA moved towards the left side of the plot due to increasing influences from *m/z* 80, *m/z* 94 ($C_2H_6S_2^+$), *m/z* 95, and *m/z* 96 (**Fig. S7**). Because the OA signal of *m/z* 80 is directly calculated from *m/z* 94 (Allan et al., 2004), we did not investigate the sources of *m/z* 80. ~~A potential source of these distinct ions in July~~In July, a potential source of these distinct ions ~~is~~ was some oxidation products of dimethyl disulphide, which shows signals at *m/z* 94, *m/z* 95, and *m/z* 96 (NIST Mass Spectrometry Data Center, 2014). Dimethyl disulphide is widely used in pesticides. Considering that the sampling site is in the middle of a farmland, and the diurnal variation of *m/z* 94 appeared to ~~have peaks~~ peak during the daytime, we considered the LO-OOA in July to be highly affected by ~~the~~ agricultural activities. However, the static factor profiles of summer LO-OOA from the seasonal summer solution had much smaller intensities for *m/z* 80 and *m/z* 94 (**Fig.** ~~**S6**~~**S4**), which enhanced the scaled residuals for these two variables in the seasonal solutions.

In winter, LO-OOA (**Fig. 9**~~**Fig. 9**~~**b**) was highly affected by biomass burning emissions ~~characterized~~ characterised by the presence of *m/z* 60, 73 (Alfarra et al., 2007), and the LO-OOA position in the f_{44} vs f_{43} space moved towards the ~~right top~~top right direction in the plot due to the increasing biogenic influence as the temperature rose (**Fig. 7**~~**Fig. 7**~~**b**, **Fig. S9**) (Canonaco et al., 2015).

Fig. 7~~**Figure 7**~~ also highlights the advantages of rolling PMF over seasonal PMF due to its time-dependent source profiles. ~~For all the seasons, both seasonal and rolling results show that the linear combinations of OOA factors could properly explain most of the measured OOA point~~Both seasonal and rolling results show that the linear combinations of OOA factors could adequately explain most of the measured OOA points for all the seasons. However, with the static OOA factors for seasonal PMF solutions, it remains ~~difficult~~ challenging to capture the variabilities of some measured data points~~, while~~. In contrast, the rolling PMF OOA factors ~~are able to~~can move correspondingly with the temporal changes of the clouds, which moves the factor profiles closer to reality and potentially decreases the scaled residuals significantly (**Fig. A3**~~**Fig. A3**~~). **Figure S9** also shows the movements of LO-OOA and MO-OOA factor profiles monthly, where LO-OOA moves towards the right direction as the temperature increases, except for the two light blue squares (June and July) in **Fig. S9a**. It is clear that temperature plays an important role for the positions of LO-OOA and MO-OOA in the f_{44} vs f_{43} space due to its influences on the OOA sources (biogenic or anthropogenic) as well as the atmospheric processes, which is consistent with previous studies in Zurich (Canonaco et al., 2015).

3.3.3 Statistical and rotational uncertainties

As suggested by Canonaco et al. (2021)~~Canonaco et al. (2020)~~, combining the bootstrap resampling and the random *a*-value techniques together with the rolling mechanism, we calculated the standard deviation (σ) and the mean (μ) of the mass concentration for each data point from each OA factor in selected "good" PMF runs. We estimated the uncertainty of each OA factor using the slope of the linear fit of σ vs μ. (**Fig. 8**~~**Fig. 8**~~). Since the ~~LOA~~58-OA factor was tightly constrained with an *a*-value of 0.05, it ~~has~~ had the smallest variability (4%). Overall, we found relatively smaller errors of HOA, BBOA, and MO-OOA (i.e., 18%, 14%, and 19%, respectively) and an error of 25% for LO-OOA, which is comparable with the previous study (Canonaco et al., 2021). The errors for both the MO-OOA and the LO-OOA factor showed

some temperature dependence. However, this actually varied with time, and the errors did not significantly change when we ~~separated~~ divided the dataset into four different temperature groups. Still, data points with higher temperature tend**ed** to have larger error for the total OOA than with lower temperature (**Fig. 8~~Fig. 8~~f**). ~~This is because more complex aging processes for OOA factors at high temperature (>20 °C) can cause more variability for the OOA factors.~~ This was most likely due to the increase of biogenic emissions and the increasing photochemistry (high O_3 and NO_2 concentration) at high temperature (>20 °C), which caused the complexity of the OOA sources.

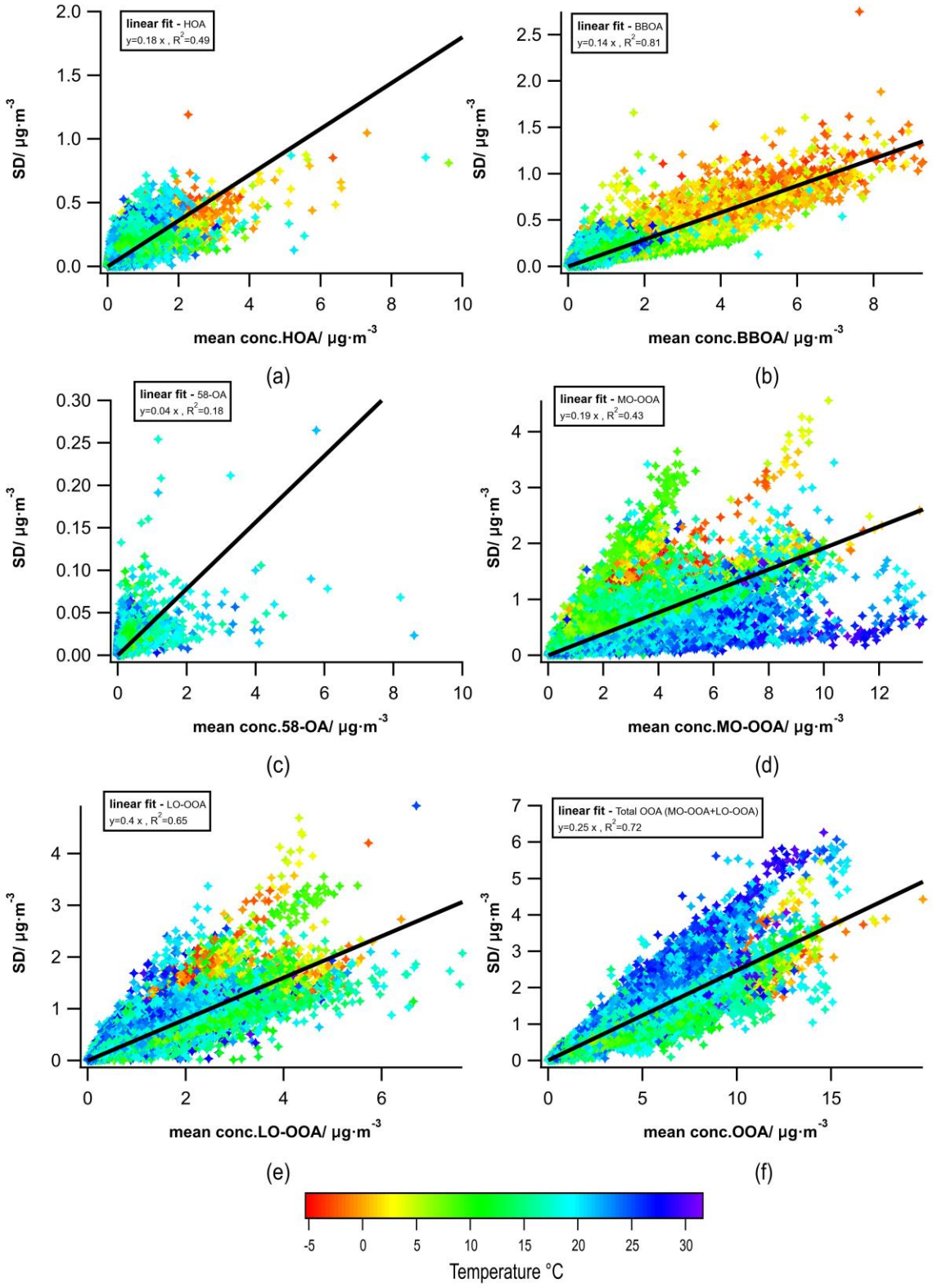

Fig. 8 Absolute statistical uncertainties of PMF for HOA, BBOA, ~~L~~58-OA, LO-OOA, MO-OOA and total OOA (LO-OOA+MO-OOA) for all data. The data points are colour-coded ~~all data points~~ by temperature. The PMF error (uncertainties) of selected PMF runs and rotational uncertainties ~~is~~are estimated using the slope of the linear regression of standard deviation (σ) vs. the averaged mass concentration (µ) for each factor.

3.3.4 Online vs. offline

The mass concentrations for HOA, BBOA~~,~~ and total OOA were compared with corresponding off~~-~~line AMS results (Vlachou et al., 2018) (**Fig. S11**). Despite some disagreement during winter (BBOA and total OOA), BBOA showed a high correlation ~~–~~with the offline results for both PM_{10} and $PM_{2.5}$, with R^2 of 0.83 and 0.84, respectively. The correlation for total OOA was somehow lower, with R^2 of 0.31 and 0.46 for the offline results of PM_{10} and $PM_{2.5}$ OOA, respectively. **Fig. 9a** shows that the rolling results had a higher OOA concentration during the winter season than the offline $PM_{2.5}/PM_{10}$ results, while the rolling results present a lower BBOA concentration during the winter season than the offline $PM_{2.5}/PM_{10}$ results (**Fig. S11b**). ~~The enhanced OOA concentration for the rolling results during winter season compared to the offline SA results (Fig. 9a), as well as the differences between the rolling results and the offline $PM_{2.5}/PM_{10}$ results regarding BBOA are most likely due to the fact that the~~As shown in **Fig. 9b,** ~~-~~ LO-OOA in the rolling results ~~was~~ were heavily affected by biomass burning with apparent biomass trace ions (i.e., *m/z* 60 and 73~~**Fig. 9b**~~). The offline results apportioned this biomass burning~~-~~ ~~–~~affected LO-OOA ~~in~~to BBOA, whereas the online ACSM measurements with a higher time resolution were capable ~~to capture~~of capturing the fast oxidation process of biomass burning sources. In addition, the rolling PMF technique enabled the LO-OOA factor profile to adapt to the temporal viabilities of OA sources, so the relatively aged biomass burning OA fraction ~~related sources~~ was apportioned into LO-OOA during winter~~-~~time by rolling PMF. Therefore, the offline AMS technique tended to underestimate OOA but overestimate BBOA in this study. The yellow line in **Fig. 9**~~**Fig. 9**~~**a** depicts the mass concentration of *m/z* 60 within LO-OOA, which clearly shows significant enhancements during winter, as well as a good agreement with the ~~LO-OOA~~ total OOA time series from the rolling results. **Figure S11** shows that HOA did not correlate at all, which ~~may be~~ is expected because

HOA is typically not ~~water~~ water-soluble, and therefore has a very low recovery rate of 0.11 for the offline AMS technique based on the ~~previous study by~~ Daellenbach et al. (2016).

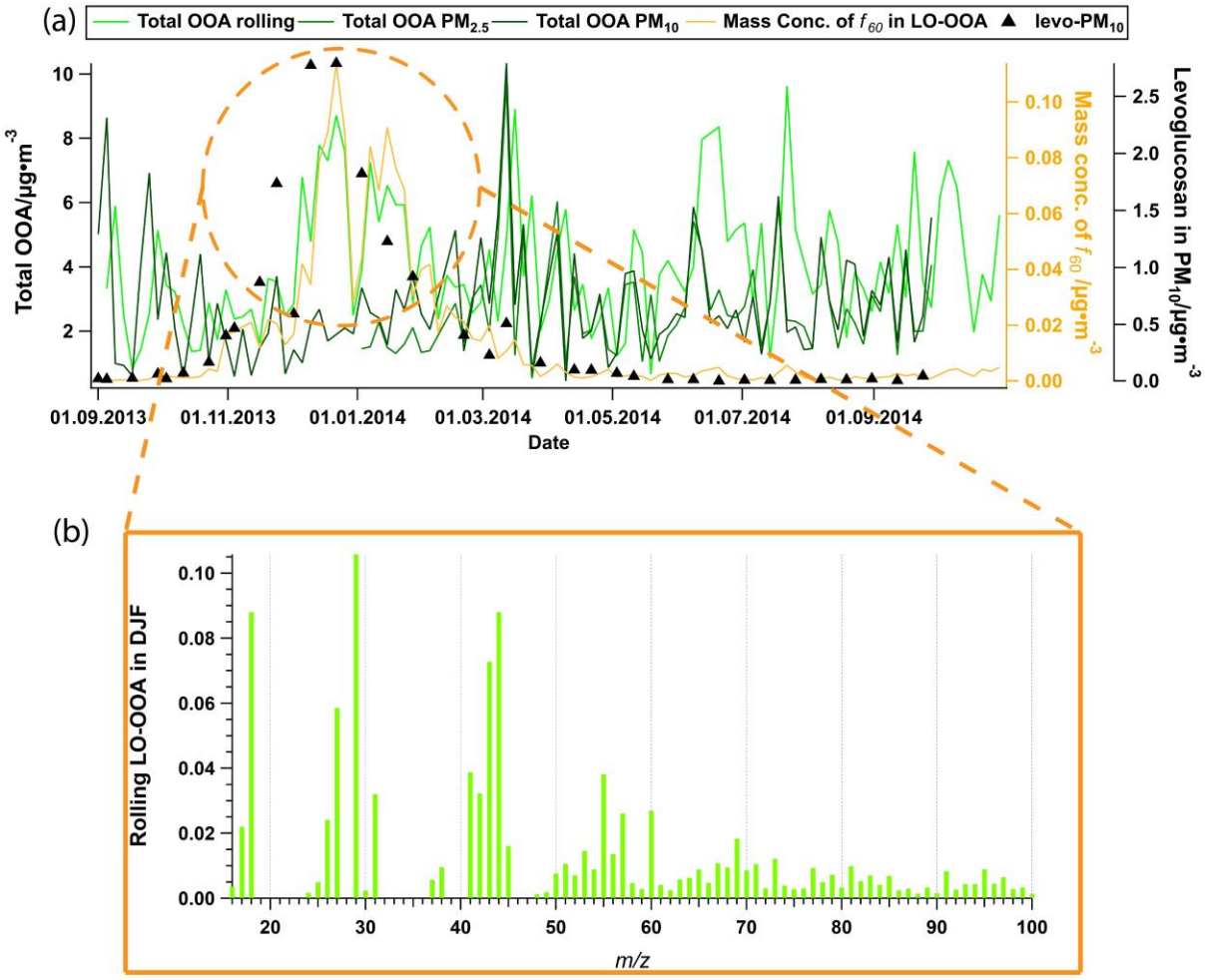

Fig. 9 (a) Time series of total oxygenated organic aerosol (LO-OOA+MO-OOA) from online and offline source apportionment solutions, together with f_{60} in LO-OOA for online solution, and levoglucosan in PM_{10} filters; (b) Averaged LO-OOA factor profile from the online solution during DJF (Dec, Jan, and Feb), when online total OOA is significantly higher than that of the offline solutions.

4 Conclusions

In this study, we conducted the first rolling PMF analysis on a 13-month ACSM data collected at a rural site ~~of~~ in Switzerland. With the help of the ~~a short~~ small rolling PMF time window ~~together with~~and the random *a*-value and bootstrap resampling analysis, we obtained a time

735 dependent SA result with error estimations. Overall, we resolved a comprehensive 5-factor
736 solution with HOA, BBOA, ~~LOA~~58-OA, MO-OOA, and LO-OOA. The contribution of HOA
737 was constant during the year (8.1–10.1%), while BBOA showed a clear seasonal variation (8.3–
738 27.4%), which peaked during winter (due to an increased residential heating source) and
739 contributed least in summer. OOA was a dominant source throughout the year, with a
740 contribution of 71.6% on a yearly average. However, the biomass burning source had a strong
741 influence on LO-OOA formation in winter. Together with BBOA, they make residential
742 heating a considerable source at Magadino during winter. Therefore, ~~a~~ mitigation of residential
743 wood combustion should be considered ~~for a reduction of~~to reduce PM levels in Magadino and
744 similar locations, especially in winter.

745 This manuscript also provided a recommended criterion list (**Table S1**) a~~s well as~~nd a novel
746 way to define thresholds with minimum subjective judgements (student's *t*-test), which could
747 be a leading example for other SoFi Pro users to conduct rolling PMF. To ensure a good
748 representation of the modelled POA factors and to validate the SA results, we also used the
749 correlations between the PMF factor time series and external data. Both HOA and BBOA
750 agreed well with the corresponding external tracers (NO_x, eBC_{tr}, and eBC_{wb}) for the yearly
751 cycles, except for summer. This is because the aethalometer model for eBC SA has higher
752 uncertainties with smaller eBC_{wb} mass concentrations. Also, NO_x could originate from multiple
753 sources in this season. Therefore, we used HOA vs~~.~~ eBC and $EV_{60,BBOA}$ to justify these two
754 factors in summer. The correlation of HOA vs eBC had an R^2 of 0.28, with an $EV_{60,BBOA}$ of
755 0.55 in summer. Moreover, the MO-OOA and LO-OOA factors were well correlated ~~well~~ with
756 inorganic SO_4 and NO_3, respectively. The identified primary and secondary OA factor profiles
757 were consistent with the OA factors previously found at ~~a variety of~~various urban, rural, and
758 remote European locations.

This paper assessed the statistical and rotational uncertainties of the PMF solution by combining the bootstrap resampling technique and the random *a*-value approach. It shows relatively small errors for constrained factors compared with a previous study in Zurich (Canonaco et al., 2021)~~,~~ and comparable errors for the OOA factors.

We also presented a head-to-head comparison between seasonal PMF solutions and the rolling PMF solution. The POA factors showed good agreement between seasonal and rolling PMF solution, while the OOA factors exhibited greater differences. Overall, the rolling PMF ~~retrieved a somewhat better solution~~provided slightly better agreements ~~in terms of agreement~~ with external tracers, especially~~, but much better correlations~~ between the OOA factors and corresponding inorganic salts. In addition, the rolling PMF results provided ~~more~~ a better representation of the measurements~~realistic results~~ by adapting the temporal variations of OOA factors in the f_{44} vs f_{43} space, which also led to much smaller scaled residuals than for the seasonal PMF. Therefore, the rolling PMF is highly useful when the user wishes to better separate OOA factors (especially during cold seasons) and better represent the measurements. In addition, we will also recommend using the rolling PMF to facilitate the analysis of long-term trends of OA sources with some prior knowledge of OA sources. However, it remains challenging to objectively define the transition point to an improved source apportionment for rolling PMF analysis when a different number of OA factors is necessary for different periods. ~~U~~An upcoming manuscript (Via et al., in prep.) will present more details of the comparison between rolling and seasonal results for multiple datasets. The time series of BBOA and total OOA agreed well with those from offline AMS ~~AS~~ SA results (Vlachou et al., 2018), except for winter when the ~~fast oxidation processes of biomass burning emissions were not captured by the offline AMS technique~~offline AMS technique did not capture the fast oxidation processes of biomass burning emissions.

Knowledge of diurnal, seasonal and annual changes in OA sources is essential for interpreting the yearly cycles of OA and defining mitigation strategies for air quality. With the help of more accurate and realistic OA sources together with an estimation of the statistical uncertainty of PMF, more constraints can be provided both for climate and air quality models. These improved results are therefore highly valuable for policy–makers to solve aerosol-related environmental issues.

5 Appendix A: Comparison between seasonal and rolling PMF solutions

The bootstrapped seasonal PMF solutions were compared with the ~~full~~ full-year rolling PMF results as follows. ~~For each factor, the correlations with external data, the ion intensities in the factor profiles, and the mass concentrations retrieved from the two different source apportionment techniques were compared~~The correlations with external data, the ion intensities in the factor profiles and the mass concentrations retrieved from the two different source apportionment techniques were compared for each factor. The correlations of the factor time series with external data (i.e., NO_x, eBC_{tr}, eBC_{wb}, eBC_{totoal}, SO_4, NO_3, and NH_4) are presented in **Table A1**~~**Table A1**~~. The rolling results ~~showed generally~~generally showed slightly better correlations between LO-OOA and NO_3, MO-OOA and SO_4, and total OOA with NH_4 than the seasonal PMF results, which is consistent with the comparison results from Canonaco et al. (2021)~~Canonaco et al. (2020)~~. A significant improvement was evident for LO-OOA vs NO_3 in spring (with R^2 increasing from 0.02 to 0.48). Concerning the correlations of POA factors with external data, rolling results and seasonal showed similar results

Table A1 Correlation coefficients ($R^2_{pearson}$) between the factor contributions and expected tracers over the year and for individual meteorological seasons (p<0.05).

Factor	Yearly		SON_2013		DJF		MAM		JJA		SON_2014	
	Seasonal	Rolling	Seasonal	Rolling	Seasonal	Rolling	Seasonal	Rolling	Seasonal	Rolling	Seasonal	Rolling
HOA / NO_x	0.37	0.35	0.52	0.5	0.46	0.47	0.34	0.36	0.15	0.15	0.44	0.42
HOA / eBC_{tr}	0.34	0.33	0.29	0.35	0.41	0.42	0.39	0.31	N/A	N/A	0.38	0.39
HOA / eBC	0.55	0.51	0.79	0.77	0.77	0.73	0.5	0.41	0.29	0.28	0.5	0.47
BBOA / eBC_{wb}	0.82	0.82	0.81	0.79	0.84	0.81	0.67	0.6	N/A	N/A	0.3	0.27
MO-OOA / SO_4^{2-}	0.58	0.49	0.49	0.61	0.52	0.49	0.62	0.66	0.63	0.57	0.43	0.46
LO-OOA / NO_3^-	0.11	0.32	0.28	0.42	0.28	0.23	0.02	0.48	0.33	0.36	0.19	0.29
OOA/ NH_4^+	0.46	0.44	0.52	0.55	0.34	0.26	0.73	0.75	0.48	0.47	0.57	0.59

As shown in **Fig. A1Figure. A1** , which shows showed a good agreement for two techniques, except for MO-OOA and LO-OOA. In general, the slope of 1.09 for rolling total OOA vs seasonal OOA suggests a slight underestimation of the OOA contribution by the seasonal PMF solutions, while the slope (<1) for HOA and BBOA suggests that the seasonal PMF solutions overestimate HOA and BBOA. In addition, LOA58-OA shows the best agreement between the seasonal and rolling solutions, due to the tight constraint of LOA58-OA with an *a*-value of 0.05.

The LO-OOA and MO-OOA factors showed worse agreement than the POA factors for the whole dataset. They had good correlations in each meteorological season, however, with different slopes. For instance, seasonal PMF underestimated LO-OOA in spring and fall 2014, but both seasons showed a high correlation with rather narrow scattering. The underestimation of LO-OOA by seasonal PMF was compensated by the overestimation of MO-OOA for these two seasons, therefore, the summed OOA still showed a high correlation between rolling and seasonal PMF results. This is expected, as the rolling PMF allows the source profiles to adapt to temporal variations, while seasonal PMF only has static source profiles.

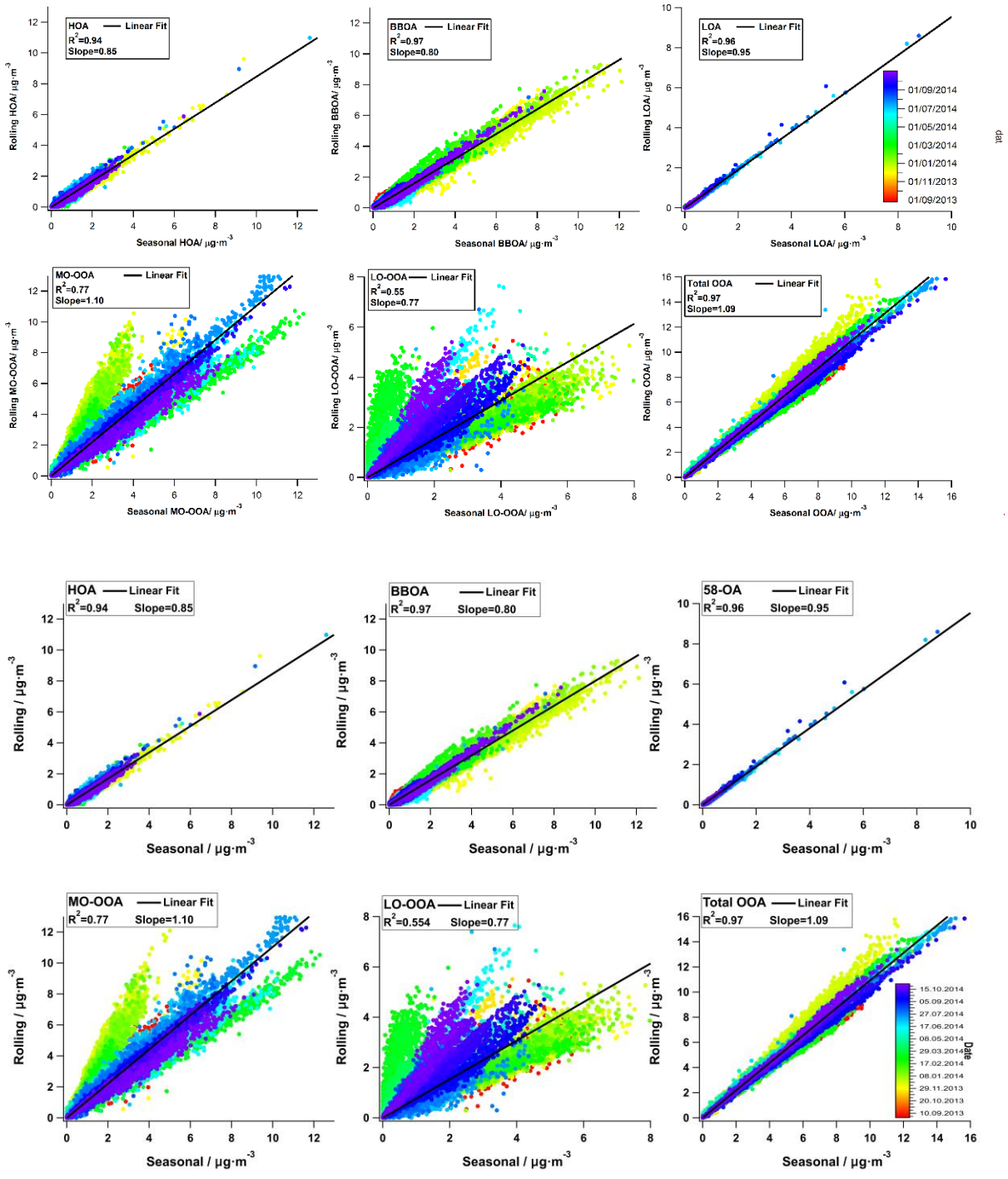

Fig. A1 Comparison of the mass concentrations resulting from rolling PMF and from the seasonal analysis for each factor (colour coded by date and time).

The differences in the major variables of the OOA factors (i.e., *m/z* 44, 43, and 60) shifted the mass concentrations significantly. Therefore, we also compared the factor profiles for both

techniques (**Fig. A2**~~**Fig. A2**~~). For instance, LO-OOA during spring showed higher intensity at *m/z* 44 for the rolling PMF results than for the seasonal PMF results (**Fig. A2**~~**Fig. A2**~~), which caused the underestimation of LO-OOA for the seasonal PMF in spring. When we averaged the total OOA factor using mass-weighted MO-OOA and LO-OOA factors, rolling PMF yielded higher *m/z* 60 for all seasons. As a result, seasonal PMF slightly underestimated the summed OOA factors by around 9%~~,~~ but slightly overestimated the POA factors by less than <6%.

The profiles of the constrained factors (HOA, BBOA, ~~LOA~~58-OA) from the rolling results show very high correlation with the seasonal results (**Fig. A2**~~**Fig. A2**~~), which suggests that the primary factors and the tightly constrained factor (~~LOA~~58-OA) were consistent with the static profiles from the seasonal PMF analysis.

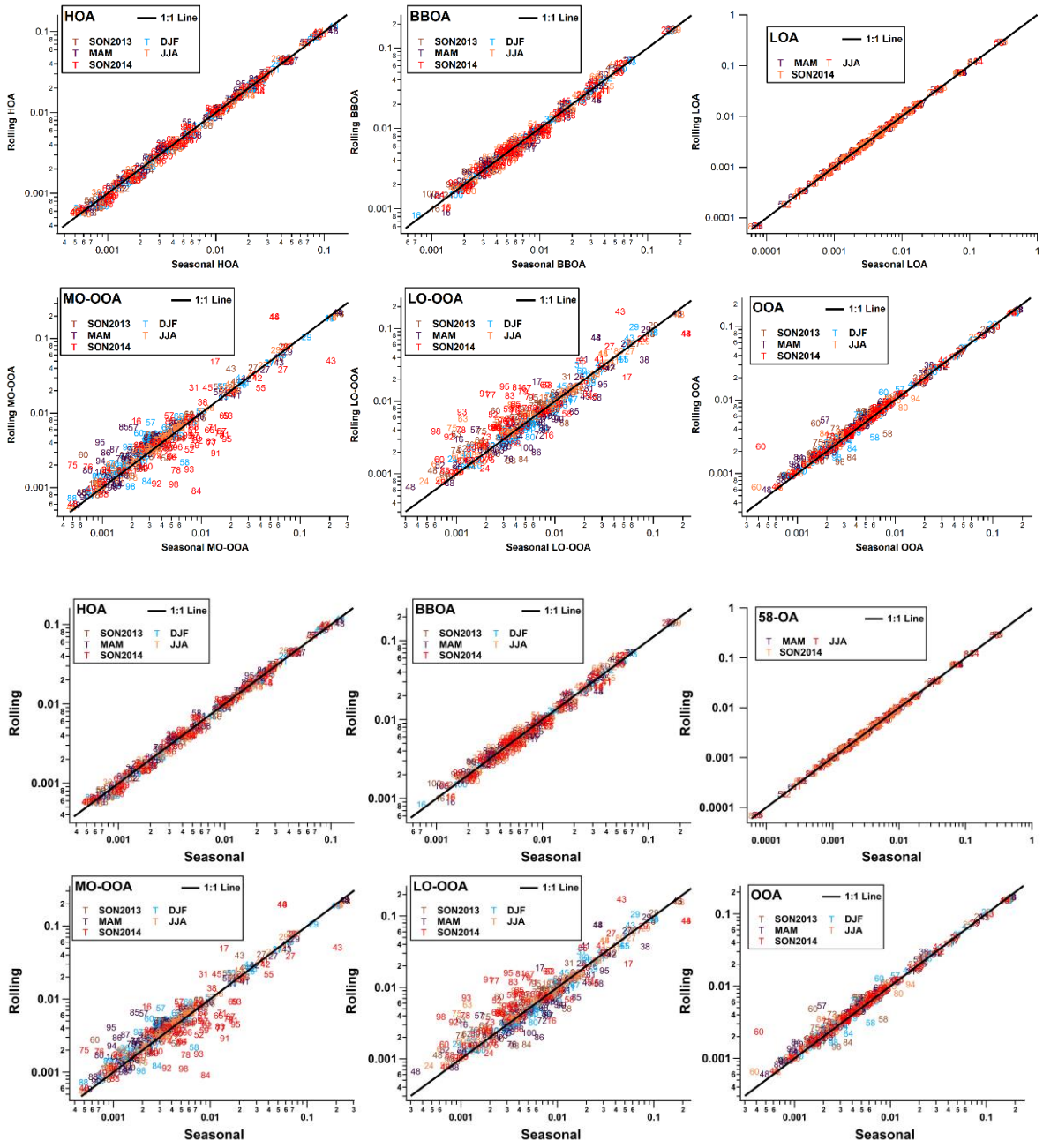

Fig. A2 Profile comparisons between rolling results and seasonal results for each factor (log scale).

We compared the scaled residuals from both source apportionment techniques (Fig. A3~~Fig. A3~~). The rolling PMF solution had smaller scaled residuals (narrower histogram and the centre was closer to 0) than that of the seasonal PMF solution, which is expected because rolling PMF had more flexibility to adapt to the temporal variabilities of the OA sources.

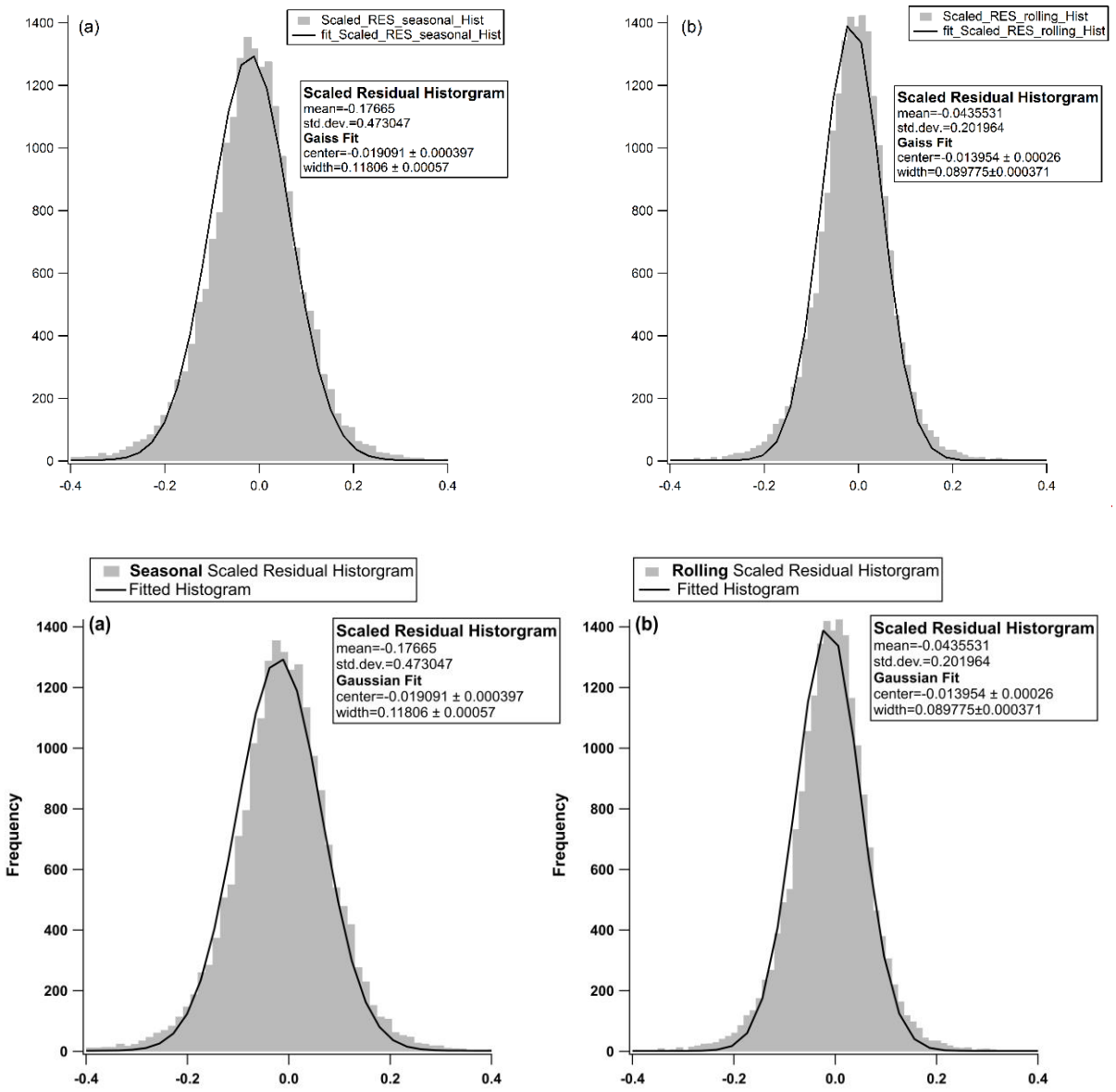

Fig. A3 Distribution of the scaled residuals over the whole year for the seasonal solution (a) and the rolling solution (b).

~~Summarizing~~Summarising, HOA and BBOA were consistent for ~~both~~ rolling and seasonal PMF analysis in terms of the time series, correlations with external tracers, and factor profiles due to the consistency of their chemical factor profiles. In contrast, the MO-OOA and LO-OOA factors were more scattered in ~~terms of averaged factor profiles and mass concentration, which suggests~~averaged factor profiles and mass concentration, suggesting that seasonal PMF

analysis was not sufficient to capture these temporal variabilities of their oxidation processes. Also, rolling PMF showed smaller scaled residuals. Therefore, we conclude that the rolling PMF analysis provides more realistic results than the seasonal analysis.

Data Availability

~~The data are available upon request to the corresponding author.~~Data related to this manuscript are available at https://zenodo.org/record/5113896 (Chen et al., 2021).

Competing interests

Y. S., F. C., A. T. K., C. B. are working for Datalystica Ltd., the company that developed the SoFi Pro software. All authors declare no competing interests in any form for this work.

~~The authors declare no competing interests in any form for this work.~~

Author contributions

G. C. analysed the ACSM and BC data, then performed the rolling source apportionment and wrote the manuscript. Y. S. wrote the preliminary manuscript and analysed preliminary results. G. C., Y. S., F. C., A. T., K. R. D., J. G. S., I. EI. H., U. B., and A. S. H. P. helped editing and reviewing the manuscript. Y. S, R. F. and P. G. helped to run the campaign. P. G., and C. H. provided external data to validate PMF solution. F.C. provided technique support for SoFi Pro. F.C., A. T., K. R. D., A. V., J. G. S., I. EI. H., U. B., and A. S. H. P. participated in discussions for this study.

~~G. C. and Y. S. contributed equally for this manuscript. G. C. wrote the manuscript, illustrations as well as data treatments and processing. Y.S. wrote the preliminary manuscript and analysed preliminary results. R. F. and P. G. helped to run the campaign. P. G., and C. H. provided external data to validate PMF solution. F.C. provided technique support for SoFi Pro. F.C., A.~~

~~T., K. R. D., A. V., J.G.S., I. EI. H., U. B., and A. S. H. P. participated discussions for this study.~~

Acknowledgements

The ACSM measurements were supported by the Swiss Federal Office for the Environment (FOEN). The leading role of the Environmental group of the Swiss Federal Laboratories for Materials and Testing (Empa) in supporting the measurements is very much appreciated. Y. S. acknowledges supports by the "Wiedereinsteigerinnen Program" at the Paul Scherrer Institute. This study was also supported by the cost action of Chemical On-Line cOmpoSition and Source Apportionment of fine aerosol (COLOSSAL, CA16109), a COST related project of the Swiss National Science Foundation, Source apportionment using long-term Aerosol Mass Spectrometry and Aethalometer Measurements (SAMSAM, IZCOZ0_177063), as well as the EU Horizon 2020 Framework Programme via the ERA-PLANET project SMURBS (grant agreement no. 689443).

References

Aiken, A. C., Salcedo, D., Cubison, M. J., Huffman, J. A., DeCarlo, P. F., Ulbrich, I. M., Docherty, K. S., Sueper, D., Kimmel, J. R., Worsnop, D. R., Trimborn, A., Northway, M., Stone, E. A., Schauer, J. J., Volkamer, R. M., Fortner, E., de Foy, B., Wang, J., Laskin, A., Shutthanandan, V., Zheng, J., Zhang, R., Gaffney, J., Marley, N. A., Paredes-Miranda, G., Arnott, W. P., Molina, L. T., Sosa, G. and Jimenez, J. L.: Mexico City aerosol analysis during MILAGRO using high resolution aerosol mass spectrometry at the urban supersite (T0) – Part 1: Fine particle composition and organic source apportionment, Atmos. Chem. Phys., 9(17), 6633–6653, doi:10.5194/acp-9-6633-2009, 2009.

Alfarra, M. R., Prevot, A. S. H., Szidat, S., Sandradewi, J., Weimer, S., Lanz, V. A., Schreiber,

907 D., Mohr, M. and Baltensperger, U.: Identification of the Mass Spectral Signature of Organic
908 Aerosols from Wood Burning Emissions, Environ. Sci. Technol., 41(16), 5770–5777,
909 doi:10.1021/es062289b, 2007.

910 Allan, J. D., Delia, A. E., Coe, H., Bower, K. N., Alfarra, M. R. R., Jimenez, J. L., Middlebrook,
911 A. M., Drewnick, F., Onasch, T. B., Canagaratna, M. R., Jayne, J. T. and Worsnop, D. R.: A
912 generalised method for the extraction of chemically resolved mass spectra from Aerodyne
913 aerosol mass spectrometer data, J. Aerosol Sci., 35(7), 909–922,
914 doi:10.1016/j.jaerosci.2004.02.007, 2004.

915 Bressi, M., Cavalli, F., Belis, C. A., Putaud, J.-P. P., Fröhlich, R., Martins dos Santos, S.,
916 Petralia, E., Prévôt, A. S. H. H., Berico, M., Malaguti, A. and Canonaco, F.: Variations in the
917 chemical composition of the submicron aerosol and in the sources of the organic fraction at a
918 regional background site of the Po Valley (Italy), Atmos. Chem. Phys., 16(20), 12875–12896,
919 doi:10.5194/acp-16-12875-2016, 2016.

920 Brown, S. S., Dibb, J. E., Stark, H., Aldener, M., Vozella, M., Whitlow, S., Williams, E. J.,
921 Lerner, B. M., Jakoubek, R., Middlebrook, A. M., DeGouw, J. A., Warneke, C., Goldan, P. D.,
922 Kuster, W. C., Angevine, W. M., Sueper, D. T., Quinn, P. K., Bates, T. S., Meagher, J. F.,
923 Fehsenfeld, F. C. and Ravishankara, A. R.: Nighttime removal of NO x in the summer marine
924 boundary layer, Geophys. Res. Lett., 31(7), n/a-n/a, doi:10.1029/2004GL019412, 2004.

925 Canagaratna, M. R., Jayne, J. T., Jimenez, J. L., Allan, J. D., Alfarra, M. R., Zhang, Q., Onasch,
926 T. B., Drewnick, F., Coe, H., Middlebrook, A., Delia, A., Williams, L. R., Trimborn, A. M.,
927 Northway, M. J., DeCarlo, P. F., Kolb, C. E., Davidovits, P. and Worsnop, D. R.: Chemical
928 and microphysical characterization of ambient aerosols with the aerodyne aerosol mass
929 spectrometer, Mass Spectrom. Rev., 26(2), 185–222, doi:10.1002/mas.20115, 2007.

930 Canonaco, F., Crippa, M., Slowik, J. G., Baltensperger, U. and Prévôt, A. S. H. H.: SoFi, an
931 IGOR-based interface for the efficient use of the generalized multilinear engine (ME-2) for the
932 source apportionment: ME-2 application to aerosol mass spectrometer data, Atmos. Meas.
933 Tech., 6(12), 3649–3661, doi:10.5194/amt-6-3649-2013, 2013.

934 Canonaco, F., Slowik, J. G., Baltensperger, U. and Prévôt, A. S. H.: Seasonal differences in
935 oxygenated organic aerosol composition: implications for emissions sources and factor
936 analysis, Atmos. Chem. Phys., 15(12), 6993–7002, doi:10.5194/acp-15-6993-2015, 2015.

937 Canonaco, F., Tobler, A., Chen, G., Sosedova, Y., Slowik, J. G. G., Bozzetti, C., Daellenbach,
938 K. R., El Haddad, I., Crippa, M., Huang, R.-J., Furger, M., Baltensperger, U., Prévôt, A. S. H.,
939 Kaspar Rudolf Haddad, I. E. D., Crippa, M., Huang, R.-J., Furger, M., Baltensperger, U.,
940 Prevot, A. S. H., Daellenbach, Kaspar Rudolf Haddad, I. El, Crippa, M., Huang, R.-J., Furger,
941 M., Baltensperger, U. and Prevot, A. S. H.: A new method for long-term source apportionment
942 with time-dependent factor profiles and uncertainty assessment using SoFi Pro: application to
943 1 year of organic aerosol data, Atmos. Meas. Tech., 14(2), 923–943, doi:10.5194/amt-14-923-
944 2021, 2021.

945 Chirico, R., DeCarlo, P. F., Heringa, M. F., Tritscher, T., Richter, R., Prévôt, A. S. H., Dommen,
946 J., Weingartner, E., Wehrle, G., Gysel, M., Laborde, M. and Baltensperger, U.: Impact of
947 aftertreatment devices on primary emissions and secondary organic aerosol formation potential
948 from in-use diesel vehicles: results from smog chamber experiments, Atmos. Chem. Phys.,
949 10(23), 11545–11563, doi:10.5194/acp-10-11545-2010, 2010.

950 Chow, J. C., Bachmann, J. D., Wierman, S. S. G., Mathai, C. V., Malm, W. C., White, W. H.,
951 Mueller, P. K., Kumar, N. and Watson, J. G.: Visibility: Science and Regulation, J. Air Waste
952 Manage. Assoc., 52(9), 973–999, doi:10.1080/10473289.2002.10470844, 2002.

Crippa, M., DeCarlo, P. F., Slowik, J. G., Mohr, C., Heringa, M. F., Chirico, R., Poulain, L., Freutel, F., Sciare, J., Cozic, J., Di Marco, C. F., Elsasser, M., Nicolas, J. B., Marchand, N., Abidi, E., Wiedensohler, A., Drewnick, F., Schneider, J., Borrmann, S., Nemitz, E., Zimmermann, R., Jaffrezo, J.-L., Prévôt, A. S. H. and Baltensperger, U.: Wintertime aerosol chemical composition and source apportionment of the organic fraction in the metropolitan area of Paris, Atmos. Chem. Phys., 13(2), 961–981, doi:10.5194/acp-13-961-2013, 2013.

Crippa, M., Canonaco, F., Lanz, V. A., Äijälä, M., Allan, J. D., Carbone, S., Capes, G., Ceburnis, D., Dall'Osto, M., Day, D. A., DeCarlo, P. F., Ehn, M., Eriksson, A., Freney, E., Hildebrandt Ruiz, L., Hillamo, R., Jimenez, J. L., Junninen, H., Kiendler-Scharr, A., Kortelainen, A.-M. M., Kulmala, M., Laaksonen, A., Mensah, A. A., Mohr, C., Nemitz, E., O'Dowd, C., Ovadnevaite, J., Pandis, S. N., Petäjä, T., Poulain, L., Saarikoski, S., Sellegri, K., Swietlicki, E., Tiitta, P., Worsnop, D. R., Baltensperger, U., Prévôt, A. S. H. H., Dall'Osto, M., Day, D. A., DeCarlo, P. F., Ehn, M., Eriksson, A., Freney, E., Hildebrandt Ruiz, L., Hillamo, R., Jimenez, J. L., Junninen, H., Kiendler-Scharr, A., Kortelainen, A.-M. M., Kulmala, M., Laaksonen, A., Mensah, A. A., Mohr, C., Nemitz, E., O'Dowd, C., Ovadnevaite, J., Pandis, S. N., Petäjä, T., Poulain, L., Saarikoski, S., Sellegri, K., Swietlicki, E., Tiitta, P., Worsnop, D. R., Baltensperger, U. and Prévôt, A. S. H. H.: Organic aerosol components derived from 25 AMS data sets across Europe using a consistent ME-2 based source apportionment approach, Atmos. Chem. Phys., 14(12), 6159–6176, doi:10.5194/acp-14-6159-2014, 2014.

Cubison, M. J. J., Ortega, A. M. M., Hayes, P. L. L., Farmer, D. K. K., Day, D., Lechner, M. J. J., Brune, W. H. H., Apel, E., Diskin, G. S., Fisher, J. A., Fuelberg, H. E., Hecobian, A., Knapp, D. J., Mikoviny, T., Riemer, D., Sachse, G. W., Sessions, W., Weber, R. J., Weinheimer, A. J., Wisthaler, A. and Jimenez, J. L.: Effects of aging on organic aerosol from open biomass burning smoke in aircraft and laboratory studies, Atmos. Chem. Phys., 11(23), 12049–12064,

978 doi:www.atmos-chem-phys.net/11/12049/2011/, 2011.

979 Daellenbach, K. R., Bozzetti, C., Křepelová, A., Canonaco, F., Wolf, R., Zotter, P., Fermo, P.,
980 Crippa, M., Slowik, J. G., Sosedova, Y., Zhang, Y., Huang, R.-J. J., Poulain, L., Szidat, S.,
981 Baltensperger, U., El Haddad, I. and Prévôt, A. S. H. H.: Characterization and source
982 apportionment of organic aerosol using offline aerosol mass spectrometry, Atmos. Meas. Tech.,
983 9(1), 23–39, doi:10.5194/amt-9-23-2016, 2016.

984 Daellenbach, K. R., Uzu, G., Jiang, J., Cassagnes, L.-E., Leni, Z., Vlachou, A., Stefenelli, G.,
985 Canonaco, F., Weber, S., Segers, A., Kuenen, J. J. P., Schaap, M., Favez, O., Albinet, A.,
986 Aksoyoglu, S., Dommen, J., Baltensperger, U., Geiser, M., El Haddad, I., Jaffrezo, J.-L. and
987 Prévôt, A. S. H.: Sources of particulate-matter air pollution and its oxidative potential in Europe,
988 Nature, 587(7834), 414–419, doi:10.1038/s41586-020-2902-8, 2020.

989 DeCarlo, P. F., Dunlea, E. J., Kimmel, J. R., Aiken, A. C., Sueper, D., Crounse, J., Wennberg,
990 P. O., Emmons, L., Shinozuka, Y., Clarke, A., Zhou, J., Tomlinson, J., Collins, D. R., Knapp,
991 D., Weinheimer, A. J., Montzka, D. D., Campos, T. and Jimenez, J. L.: Fast airborne aerosol
992 size and chemistry measurements above Mexico City and Central Mexico during the
993 MILAGRO campaign, Atmos. Chem. Phys., 8(14), 4027–4048, doi:10.5194/acp-8-4027-2008,
994 2008.

995 Dentener, F. J. and Crutzen, P. J.: Reaction of N 2 O 5 on tropospheric aerosols: Impact on the
996 global distributions of NO x , O 3 , and OH, J. Geophys. Res. Atmos., 98(D4), 7149–7163,
997 doi:10.1029/92JD02979, 1993.

998 Dockery, D. W. and Pope, C. A.: Acute Respiratory Effects of Particulate Air Pollution, Annu.
999 Rev. Public Health, 15(1), 107–132, doi:10.1146/annurev.pu.15.050194.000543, 1994.

1000 Duplissy, J., DeCarlo, P. F., Dommen, J., Alfarra, M. R., Metzger, A., Barmpadimos, I., Prevot,

A. S. H., Weingartner, E., Tritscher, T., Gysel, M., Aiken, A. C., Jimenez, J. L., Canagaratna, M. R., Worsnop, D. R., Collins, D. R., Tomlinson, J. and Baltensperger, U.: Relating hygroscopicity and composition of organic aerosol particulate matter, Atmos. Chem. Phys., 11(3), 1155–1165, doi:10.5194/acp-11-1155-2011, 2011.

Efron, B.: Bootstrap Methods: Another Look at the Jackknife, Ann. Stat., 7(1), 1–26 [online] Available from: https://www.jstor.org/stable/2958830, 1979.

Fröhlich, R., Cubison, M. J., Slowik, J. G., Bukowiecki, N., Prévôt, A. S. H. H., Baltensperger, U., Schneider, J., Kimmel, J. R., Gonin, M., Rohner, U., Worsnop, D. R. and Jayne, J. T.: The ToF-ACSM: a portable aerosol chemical speciation monitor with TOFMS detection, Atmos. Meas. Tech., 6(11), 3225–3241, doi:10.5194/amt-6-3225-2013, 2013.

Fröhlich, R., Crenn, V., Setyan, A., Belis, C. A., Canonaco, F., Favez, O., Riffault, V., Slowik, J. G., Aas, W., Aijälä, M., Alastuey, A., Artiñano, B., Bonnaire, N., Bozzetti, C., Bressi, M., Carbone, C., Coz, E., Croteau, P. L., Cubison, M. J., Esser-Gietl, J. K., Green, D. C., Gros, V., Heikkinen, L., Herrmann, H., Jayne, J. T., Lunder, C. R., Minguillón, M. C., Močnik, G., O'Dowd, C. D., Ovadnevaite, J., Petralia, E., Poulain, L., Priestman, M., Ripoll, A., Sarda-Estève, R., Wiedensohler, A., Baltensperger, U., Sciare, J., Prévôt, A. S. H., O'Dowd, C. D., Ovadnevaite, J., Petralia, E., Poulain, L., Priestman, M., Ripoll, A., Sarda-Estève, R., Wiedensohler, A., Baltensperger, U., Sciare, J., Prévôt, A. S. H., O'Dowd, C. D., Ovadnevaite, J., Petralia, E., Poulain, L., Priestman, M., Ripoll, A., Sarda-Estève, R., Wiedensohler, A., Baltensperger, U., Sciare, J. and Prévôt, A. S. H.: ACTRIS ACSM intercomparison – Part 2: Intercomparison of ME-2 organic source apportionment results from 15 individual, co-located aerosol mass spectrometers, Atmos. Meas. Tech., 8(6), 2555–2576, doi:10.5194/amt-8-2555-2015, 2015.

Heringa, M. F., DeCarlo, P. F., Chirico, R., Tritscher, T., Dommen, J., Weingartner, E., Richter,

1025 R., Wehrle, G., Prévôt, A. S. H. and Baltensperger, U.: Investigations of primary and secondary
1026 particulate matter of different wood combustion appliances with a high-resolution time-of-
1027 flight aerosol mass spectrometer, Atmos. Chem. Phys., 11(12), 5945–5957, doi:10.5194/acp-
1028 11-5945-2011, 2011.

1029 Hildebrandt, L., Kostenidou, E., Lanz, V. A., Prevot, A. S. H. H., Baltensperger, U.,
1030 Mihalopoulos, N., Laaksonen, A., Donahue, N. M. and Pandis, S. N.: Sources and atmospheric
1031 processing of organic aerosol in the Mediterranean: insights from aerosol mass spectrometer
1032 factor analysis, Atmos. Chem. Phys., 11(23), 12499–12515, doi:10.5194/acp-11-12499-2011,
1033 2011.

1034 Horvath, H.: Atmospheric light absorption—A review, Atmos. Environ. Part A. Gen. Top.,
1035 27(3), 293–317, doi:10.1016/0960-1686(93)90104-7, 1993.

1036 IPCC: Clouds and Aerosols, in Climate Change 2013 - The Physical Science Basis, edited by
1037 Intergovernmental Panel on Climate Change, pp. 571–658, Cambridge University Press,
1038 Cambridge., 2014.

1039 Jacobson, M. C., Hansson, H.-C., Noone, K. J. and Charlson, R. J.: Organic atmospheric
1040 aerosols: Review and state of the science, Rev. Geophys., 38(2), 267–294,
1041 doi:10.1029/1998RG000045, 2000.

1042 Jacobson, M. Z.: Global direct radiative forcing due to multicomponent anthropogenic and
1043 natural aerosols, J. Geophys. Res. Atmos., 106(D2), 1551–1568, doi:10.1029/2000JD900514,
1044 2001.

1045 Jimenez, J. L., Canagaratna, M. R., Donahue, N. M., Prevot, A. S. H. H., Zhang, Q., Kroll, J.
1046 H., DeCarlo, P. F., Allan, J. D., Coe, H., Ng, N. L., Aiken, A. C., Docherty, K. S., Ulbrich, I.
1047 M., Grieshop, A. P., Robinson, A. L., Duplissy, J., Smith, J. D., Wilson, K. R., Lanz, V. A.,

1048 Hueglin, C., Sun, Y. L., Tian, J., Laaksonen, A., Raatikainen, T., Rautiainen, J., Vaattovaara,
1049 P., Ehn, M., Kulmala, M., Tomlinson, J. M., Collins, D. R., Cubison, M. J., Dunlea, E. J.,
1050 Huffman, J. A., Onasch, T. B., Alfarra, M. R., Williams, P. I., Bower, K., Kondo, Y., Schneider,
1051 J., Drewnick, F., Borrmann, S., Weimer, S., Demerjian, K., Salcedo, D., Cottrell, L., Griffin,
1052 R., Takami, A., Miyoshi, T., Hatakeyama, S., Shimono, A., Sun, J. Y., Zhang, Y. M., Dzepina,
1053 K., Kimmel, J. R., Sueper, D., Jayne, J. T., Herndon, S. C., Trimborn, A. M., Williams, L. R.,
1054 Wood, E. C., Middlebrook, A. M., Kolb, C. E., Baltensperger, U., Worsnop, D. R., Dunlea, J.,
1055 Huffman, J. A., Onasch, T. B., Alfarra, M. R., Williams, P. I., Bower, K., Kondo, Y., Schneider,
1056 J., Drewnick, F., Borrmann, S., Weimer, S., Demerjian, K., Salcedo, D., Cottrell, L., Griffin,
1057 R., Takami, A., Miyoshi, T., Hatakeyama, S., Shimono, A., Sun, J. Y., Zhang, Y. M., Dzepina,
1058 K., Kimmel, J. R., Sueper, D., Jayne, J. T., Herndon, S. C., Trimborn, A. M., Williams, L. R.,
1059 Wood, E. C., Middlebrook, A. M., Kolb, C. E., Baltensperger, U., Worsnop, D. R., Dunlea, E.
1060 J., Huffman, J. A., et al.: Evolution of organic aerosols in the atmosphere, Science (80-.).,
1061 326(5959), 1525–1529, doi:10.1126/science.1180353, 2009.

1062 Lanz, V. A., Alfarra, M. R., Baltensperger, U., Buchmann, B., Hueglin, C. and Prévôt, A. S.
1063 H.: Source apportionment of submicron organic aerosols at an urban site by factor analytical
1064 modelling of aerosol mass spectra, Atmos. Chem. Phys., 7(6), 1503–1522, doi:10.5194/acp-7-
1065 1503-2007, 2007.

1066 Lanz, V. A., Alfarra, M. R., Baltensperger, U., Buchmann, B., Hueglin, C., Szidat, S., Wehrli,
1067 M. N., Wacker, L., Weimer, S., Caseiro, A., Puxbaum, H. and Prevot, A. S. H.: Source
1068 Attribution of Submicron Organic Aerosols during Wintertime Inversions by Advanced Factor
1069 Analysis of Aerosol Mass Spectra, Environ. Sci. Technol., 42(1), 214–220,
1070 doi:10.1021/es0707207, 2008.

1071 Lelieveld, J., Evans, J. S., Fnais, M., Giannadaki, D. and Pozzer, A.: The contribution of

outdoor air pollution sources to premature mortality on a global scale, Nature, 525(7569), 367–371, doi:10.1038/nature15371, 2015.

Matthew, B. M., Middlebrook, A. M. and Onasch, T. B.: Collection Efficiencies in an Aerodyne Aerosol Mass Spectrometer as a Function of Particle Phase for Laboratory Generated Aerosols, Aerosol Sci. Technol., 42(11), 884–898, doi:10.1080/02786820802356797, 2008.

Mauderly, J. L. and Chow, J. C.: Health Effects of Organic Aerosols, Inhal. Toxicol., 20(3), 257–288, doi:10.1080/08958370701866008, 2008.

Meteotest: Data Report Switzerland 2007 – 2016, Bern, Switzerland., 2017.

Minguillón, M. C., Ripoll, A., Pérez, N., Prévôt, A. S. H. H., Canonaco, F., Querol, X. and Alastuey, A.: Chemical characterization of submicron regional background aerosols in the western Mediterranean using an Aerosol Chemical Speciation Monitor, Atmos. Chem. Phys., 15(11), 6379–6391, doi:10.5194/acp-15-6379-2015, 2015.

Mohr, C., Decarlo, P. F., Heringa, M. F., Chirico, R., Slowik, J. G., Richter, R., Reche, C., Alastuey, A., Querol, X., Seco, R., Crippa, M., Zimmermann, R., Baltensperger, U., Barcelona, D., Munchen, H. Z. and Mass, J.: Wintertime aerosol chemical composition and source apportionment of the organic fraction in the metropolitan area of Paris, Atmos. Chem. Phys., 12(4), 1649–1665, doi:10.5194/acp-13-961-2013, 2012.

Monn, C.: Exposure assessment of air pollutants: a review on spatial heterogeneity and indoor/outdoor/personal exposure to suspended particulate matter, nitrogen dioxide and ozone, Atmos. Environ., 35(1), 1–32, doi:10.1016/S1352-2310(00)00330-7, 2001.

Murphy, D. M., Cziczo, D. J., Froyd, K. D., Hudson, P. K., Matthew, B. M., Middlebrook, A. M., Peltier, R. E., Sullivan, A., Thomson, D. S. and Weber, R. J.: Single-particle mass spectrometry of tropospheric aerosol particles, J. Geophys. Res. Atmos., 111(D23), n/a-n/a,

doi:10.1029/2006JD007340, 2006.

Ng, N. L., Canagaratna, M. R., Zhang, Q., Jimenez, J. L., Tian, J., Ulbrich, I. M., Kroll, J. H., Docherty, K. S., Chhabra, P. S., Bahreini, R., Murphy, S. M., Seinfeld, J. H., Hildebrandt, L., Donahue, N. M., DeCarlo, P. F., Lanz, V. A., Prévôt, A. S. H. H., Dinar, E., Rudich, Y. and Worsnop, D. R.: Organic aerosol components observed in Northern Hemispheric datasets from Aerosol Mass Spectrometry, Atmos. Chem. Phys., 10(10), 4625–4641, doi:10.5194/acp-10-4625-2010, 2010.

Ng, N. L., Herndon, S. C., Trimborn, A., Canagaratna, M. R., Croteau, P. L., Onasch, T. B., Sueper, D., Worsnop, D. R., Zhang, Q., Sun, Y. L. and Jayne, J. T.: An Aerosol Chemical Speciation Monitor (ACSM) for Routine Monitoring of the Composition and Mass Concentrations of Ambient Aerosol, Aerosol Sci. Technol., 45(7), 780–794, doi:10.1080/02786826.2011.560211, 2011a.

Ng, N. L., Canagaratna, M. R., Jimenez, J. L., Zhang, Q., Ulbrich, I. M. and Worsnop, D. R.: Real-Time Methods for Estimating Organic Component Mass Concentrations from Aerosol Mass Spectrometer Data, Environ. Sci. Technol., 45(3), 910–916, doi:10.1021/es102951k, 2011b.

NIST Mass Spectrometry Data Center: Disulfide, dimethyl, SRD 69. [online] Available from: https://webbook.nist.gov/cgi/cbook.cgi?ID=C624920&Mask=200#Refs (Accessed 6 August 2020), 2014.

Paatero, P.: The Multilinear Engine—A Table-Driven, Least Squares Program for Solving Multilinear Problems, Including the n -Way Parallel Factor Analysis Model, J. Comput. Graph. Stat., 8(4), 854–888, doi:10.1080/10618600.1999.10474853, 1999.

Paatero, P. and Hopke, P. K.: Discarding or downweighting high-noise variables in factor

analytic models, Anal. Chim. Acta, 490(1–2), 277–289, doi:10.1016/S0003-2670(02)01643-4, 2003.

Paatero, P., Eberly, S., Brown, S. G. and Norris, G. A.: Methods for estimating uncertainty in factor analytic solutions, Atmos. Meas. Tech., 7(3), 781–797, doi:10.5194/amt-7-781-2014, 2014.

Parworth, C., Fast, J., Mei, F., Shippert, T., Sivaraman, C., Tilp, A., Watson, T. and Zhang, Q.: Long-term measurements of submicrometer aerosol chemistry at the Southern Great Plains (SGP) using an Aerosol Chemical Speciation Monitor (ACSM), Atmos. Environ., 106, 43–55, doi:10.1016/j.atmosenv.2015.01.060, 2015.

Petit, J.-E. E., Favez, O., Sciare, J., Canonaco, F., Croteau, P., Močnik, G., Jayne, J., Worsnop, D. and Leoz-Garziandia, E.: Submicron aerosol source apportionment of wintertime pollution in Paris, France by double positive matrix factorization (PMF2) using an aerosol chemical speciation monitor (ACSM) and a multi-wavelength Aethalometer, Atmos. Chem. Phys., 14(24), 13773–13787, doi:10.5194/acp-14-13773-2014, 2014.

Pfaffenberger, L., Barmet, P., Slowik, J. G., Praplan, A. P., Dommen, J., Prévôt, A. S. H. and Baltensperger, U.: The link between organic aerosol mass loading and degree of oxygenation: an α-pinene photooxidation study, Atmos. Chem. Phys., 13(13), 6493–6506, doi:10.5194/acp-13-6493-2013, 2013.

Pope, C. A. and Dockery, D. W.: Health Effects of Fine Particulate Air Pollution: Lines that Connect, J. Air Waste Manage. Assoc., 56(6), 709–742, doi:10.1080/10473289.2006.10464485, 2006.

Ramanathan, V., Chung, C., Kim, D., Bettge, T., Buja, L., Kiehl, J. T., Washington, W. M., Fu, Q., Sikka, D. R. and Wild, M.: Atmospheric brown clouds: Impacts on South Asian climate

and hydrological cycle, Proc. Natl. Acad. Sci., 102(15), 5326–5333, doi:10.1073/pnas.0500656102, 2005.

Reyes-Villegas, E., Green, D. C., Priestman, M., Canonaco, F., Coe, H., Prévôt, A. S. H. H. and Allan, J. D.: Organic aerosol source apportionment in London 2013 with ME-2: Exploring the solution space with annual and seasonal analysis, Atmos. Chem. Phys., 16(24), 15545–15559, doi:10.5194/acp-16-15545-2016, 2016.

Ripoll, A., Minguillón, M. C., Pey, J., Jimenez, J. L., Day, D. A., Sosedova, Y., Canonaco, F., Prévôt, A. S. H., Querol, X. and Alastuey, A.: Long-term real-time chemical characterization of submicron aerosols at Montsec (southern Pyrenees, 1570 m a.s.l.), Atmos. Chem. Phys., 15(6), 2935–2951, doi:10.5194/acp-15-2935-2015, 2015.

von Schneidemesser, E., Monks, P. S., Allan, J. D., Bruhwiler, L., Forster, P., Fowler, D., Lauer, A., Morgan, W. T., Paasonen, P., Righi, M., Sindelarova, K. and Sutton, M. A.: Chemistry and the Linkages between Air Quality and Climate Change, Chem. Rev., 115(10), 3856–3897, doi:10.1021/acs.chemrev.5b00089, 2015.

Schurman, M. I., Lee, T., Sun, Y., Schichtel, B. A., Kreidenweis, S. M. and Collett Jr., J. L.: Investigating types and sources of organic aerosol in Rocky Mountain National Park using aerosol mass spectrometry, Atmos. Chem. Phys., 15(2), 737–752, doi:10.5194/acp-15-737-2015, 2015.

Schwarz, J. P., Gao, R. S., Perring, A. E., Spackman, J. R. and Fahey, D. W.: Black carbon aerosol size in snow, Sci. Rep., 3, 1–5, doi:10.1038/srep01356, 2013.

Sug Park, E., Henry, R. C. and Spiegelman, C. H.: Estimating the number of factors to include in a high-dimensional multivariate bilinear model, Commun. Stat. - Simul. Comput., 29(3), 723–746, doi:10.1080/03610910008813637, 2000.

1164 Szidat, S., Prévôt, A. S. H., Sandradewi, J., Alfarra, M. R., Synal, H.-A., Wacker, L. and
1165 Baltensperger, U.: Dominant impact of residential wood burning on particulate matter in
1166 Alpine valleys during winter, Geophys. Res. Lett., 34(5), doi:10.1029/2006GL028325, 2007.

1167 The Swiss Federal Council: Ordinance of 16 December 1985 on Air Pollution Control (OAPC).
1168 [online] Available from: https://www.admin.ch/opc/en/classified-
1169 compilation/19850321/index.html#app7 (Accessed 10 September 2019), 2018.

1170 Tobler, A., Bhattu, D., Canonaco, F., Lalchandani, V., Shukla, A., Thamban, N. M., Mishra,
1171 S., Srivastava, A. K., Bisht, D. S., Tiwari, S., Singh, S., Močnik, G., Baltensperger, U., Tripathi,
1172 S. N., Slowik, J. G. and Prévôt, A. S. H.: Chemical characterization of PM2.5 and source
1173 apportionment of organic aerosol in New Delhi, India, Sci. Total Environ., 745, 140924,
1174 doi:10.1016/j.scitotenv.2020.140924, 2020.

1175 Ulbrich, I. M., Canagaratna, M. R., Zhang, Q., Worsnop, D. R. and Jimenez, J. L.:
1176 Interpretation of organic components from Positive Matrix Factorization of aerosol mass
1177 spectrometric data, Atmos. Chem. Phys., 9(9), 2891–2918, doi:10.5194/acp-9-2891-2009,
1178 2009.

1179 Via, M. et al.: Comparison between rolling and seasonal PMF techniques for organic aerosol
1180 source apportionment [Unpublished manuscript]., 2021.

1181 Vlachou, A., Daellenbach, K. R., Bozzetti, C., Chazeau, B., Salazar, G. A., Szidat, S., Jaffrezo,
1182 J.-L., Hueglin, C., Baltensperger, U., Haddad, I. El and Prévôt, A. S. H.: Advanced source
1183 apportionment of carbonaceous aerosols by coupling offline AMS and radiocarbon size-
1184 segregated measurements over a nearly 2-year period, Atmos. Chem. Phys., 18(9), 6187–6206,
1185 doi:10.5194/acp-18-6187-2018, 2018.

1186 Zhang, Q., Jimenez, J. L., Canagaratna, M. R., Allan, J. D., Coe, H., Ulbrich, I., Alfarra, M. R.,

Takami, A., Middlebrook, A. M., Sun, Y. L., Dzepina, K., Dunlea, E., Docherty, K., DeCarlo, P. F., Salcedo, D., Onasch, T., Jayne, J. T., Miyoshi, T., Shimono, A., Hatakeyama, S., Takegawa, N., Kondo, Y., Schneider, J., Drewnick, F., Borrmann, S., Weimer, S., Demerjian, K., Williams, P., Bower, K., Bahreini, R., Cottrell, L., Griffin, R. J., Rautiainen, J., Sun, J. Y., Zhang, Y. M. and Worsnop, D. R.: Ubiquity and dominance of oxygenated species in organic aerosols in anthropogenically-influenced Northern Hemisphere midlatitudes, Geophys. Res. Lett., 34(13), n/a-n/a, doi:10.1029/2007GL029979, 2007.

Zhang, Q., Jimenez, J. L., Canagaratna, M. R., Ulbrich, I. M., Ng, N. L., Worsnop, D. R. and Sun, Y.: Understanding atmospheric organic aerosols via factor analysis of aerosol mass spectrometry: a review, Anal. Bioanal. Chem., 401(10), 3045–3067, doi:10.1007/s00216-011-5355-y, 2011.

Zhang, Y., Favez, O., Petit, J.-E., Canonaco, F., Truong, F., Bonnaire, N., Crenn, V., Amodeo, T., Prévôt, A. S. H., Sciare, J., Gros, V. and Albinet, A.: Six-year source apportionment of submicron organic aerosols from near-continuous highly time-resolved measurements at SIRTA (Paris area, France), Atmos. Chem. Phys., 19(23), 14755–14776, doi:10.5194/acp-19-14755-2019, 2019.

Zotter, P., Herich, H., Gysel, M., El-Haddad, I., Zhang, Y., Močnik, G., Hüglin, C., Baltensperger, U., Szidat, S., Prévôt, A. S. H. H., Mocnik, G., Hüglin, C., Baltensperger, U., Szidat, S., Prévôt, A. S. H. H., Močnik, G., Hüglin, C., Baltensperger, U., Szidat, S. and Prévôt, A. S. H. H.: Evaluation of the absorption Ångström exponents for traffic and wood burning in the Aethalometer-based source apportionment using radiocarbon measurements of ambient aerosol, Atmos. Chem. Phys., 17(6), 4229–4249, doi:10.5194/acp-17-4229-2017, 2017.

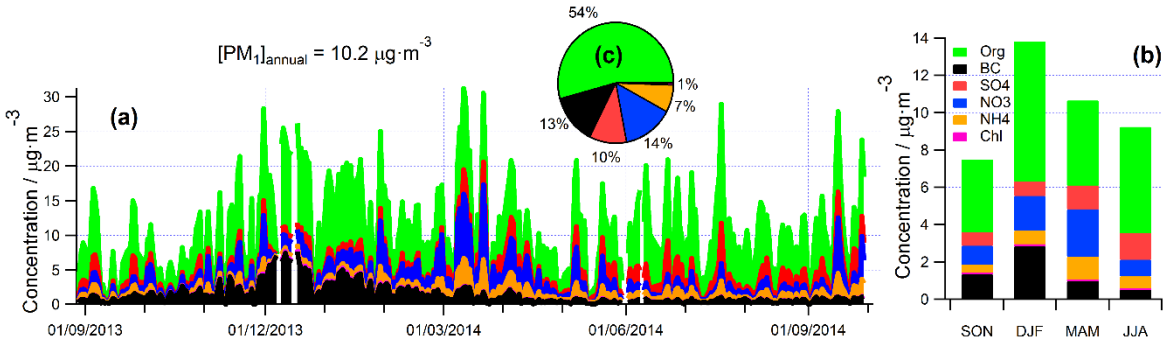

Fig. 1 Chemical composition of PM_1 in Magadino 2013-2014 – daily (a), seasonal (b) and annual (c) averages. The labels indicate the non-refractory organics (Org), sulphate (SO_4), nitrate (NO_3), ammonium (NH_4) and chloride (Cl) ions measured by ACSM, and the black carbon (BC) measured by light absorption.

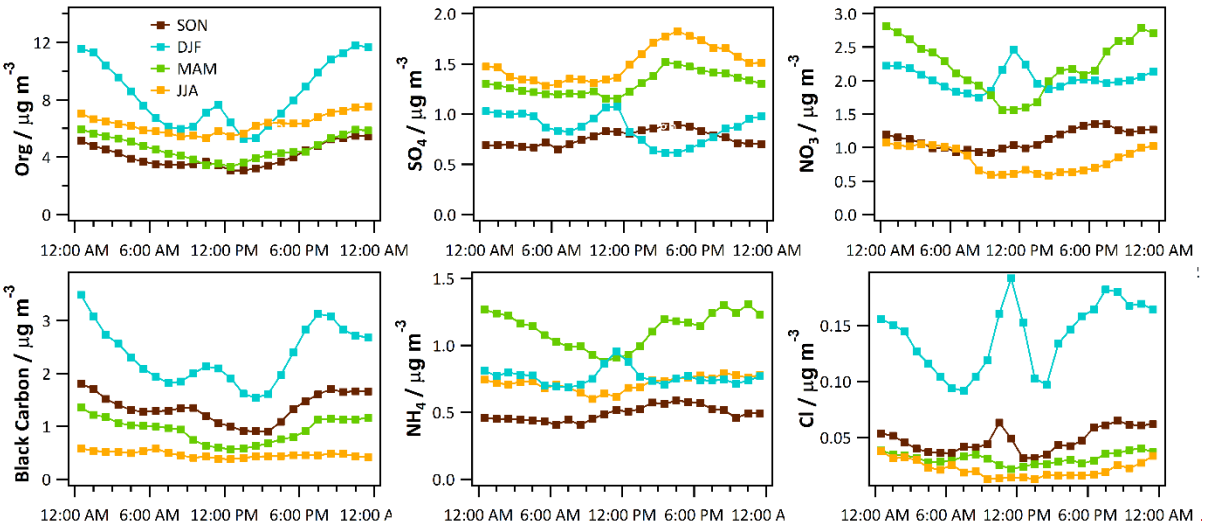

Fig. 2 Seasonal diurnal cycles of PM_1 constituents calculated as an hourly average for ACSM organic and inorganic species (sulphate, nitrate, ammonium, and chloride) and black carbon

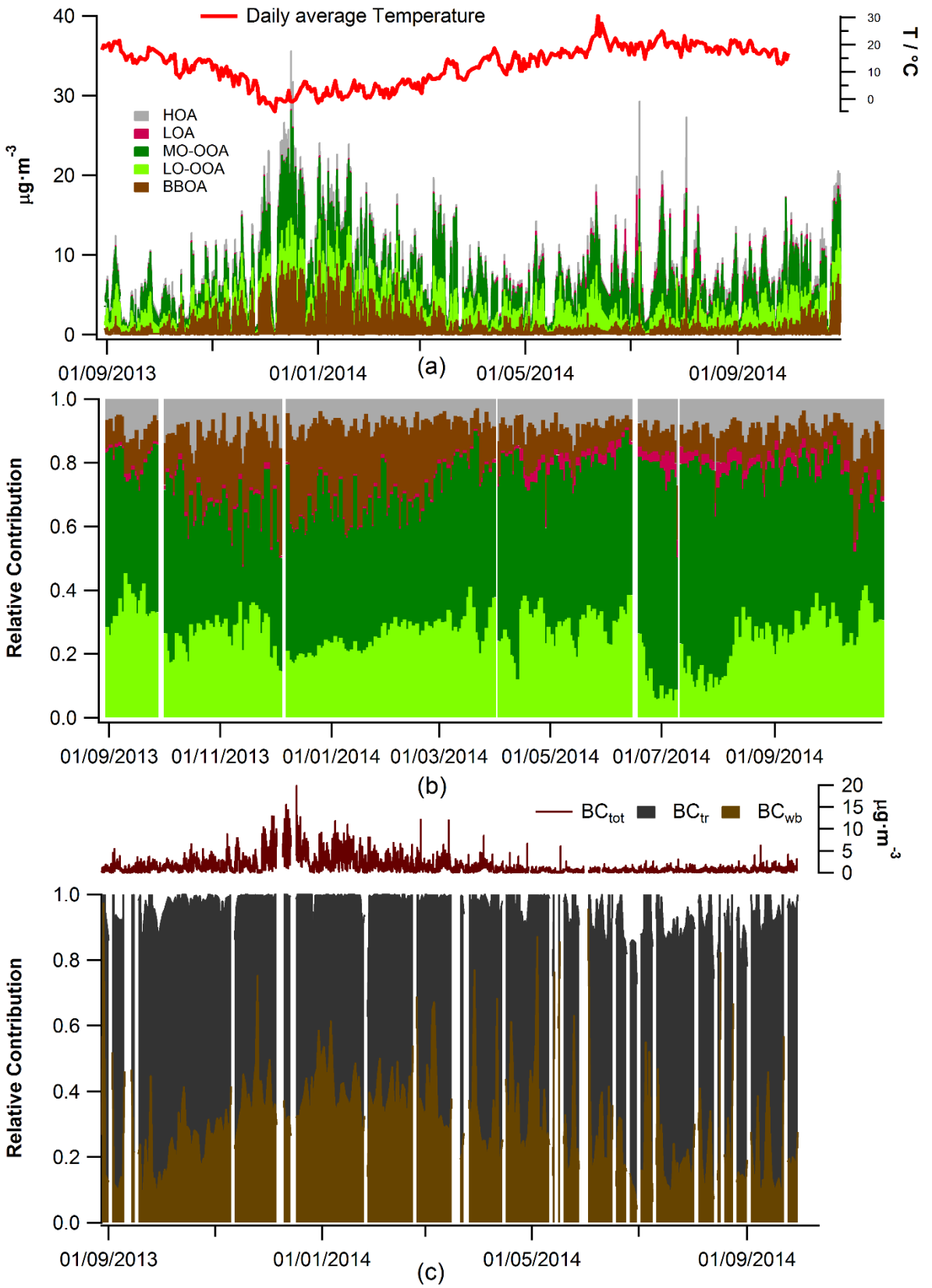

Fig. 3 Annual cycle of OA sources: (a) absolute and (b) relative OA contributions plotted as 30-min resolved time series, (c) BC source apportionment.

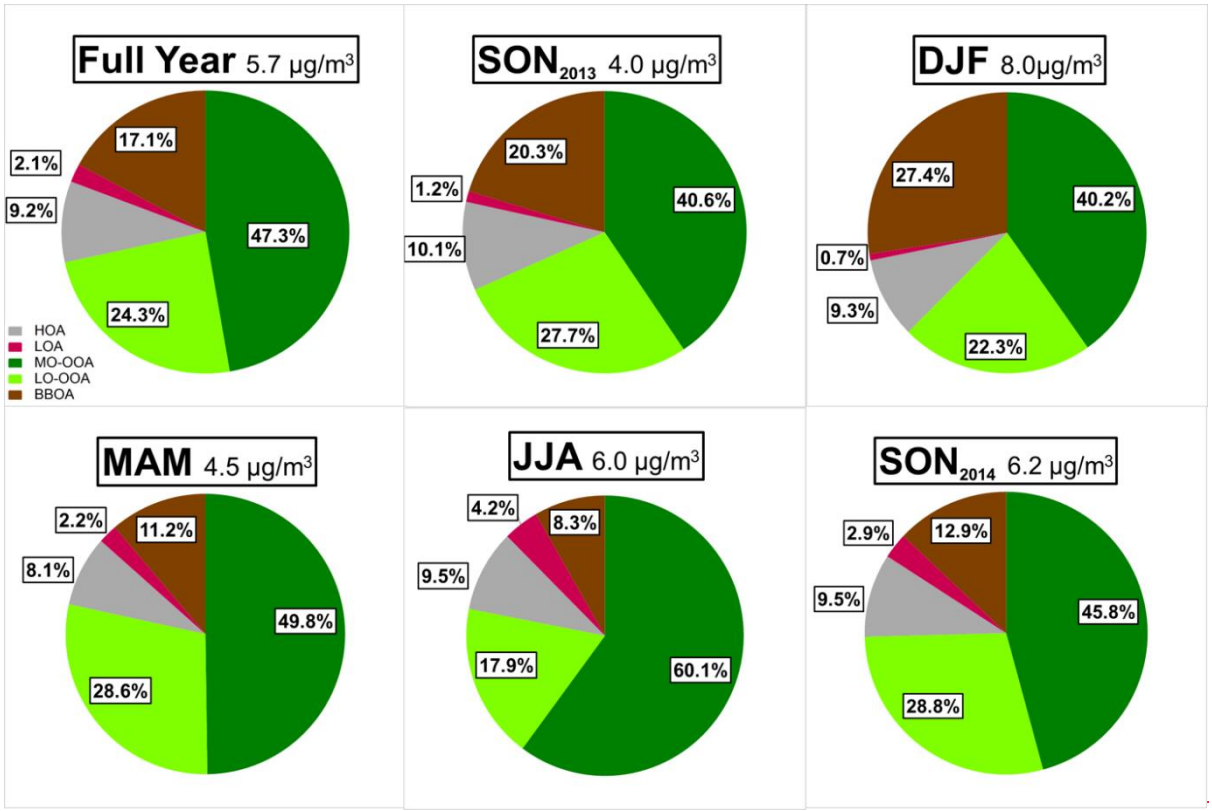

Fig. 4 OA pie charts for the whole year and for different seasons.

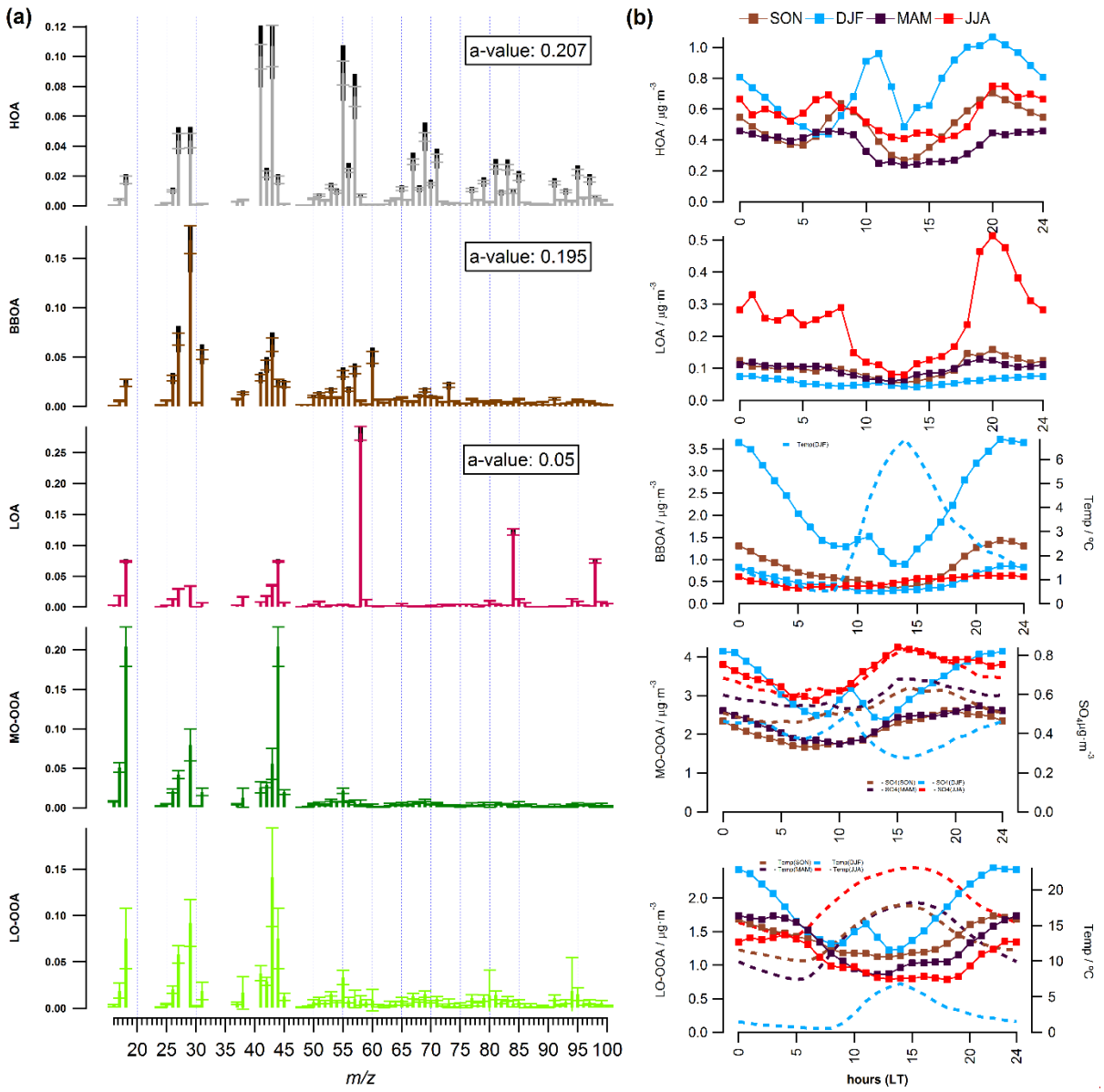

Fig. 5 Overview of the primary and secondary OA sources in Magadino in 2013-2014: (a) OA factor profiles and (b) seasonal diurnal cycles of HOA, BBOA, LOA, MO-OOA, and LO-OOA. The ambient temperature is shown on the LO-OOA diurnal plots, respectively. In (a) the error bar is the standard deviation; the black bars show the maximum and the minimum that the variable allowed to be vary from the reference profiles. The average, 10th and 90th percentiles for a-values of HOA are, 0.195, 0.007 and 0.378, respectively. Also, the average, 10th and 90th percentiles for a-values of BBOA are 0.202, 0.025 and 0.379, respectively.

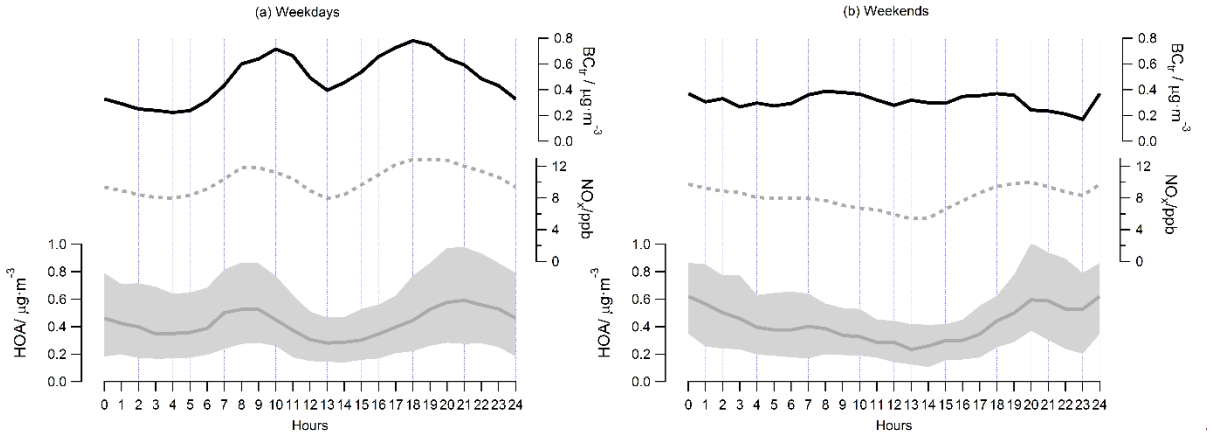

Fig. 6 Diurnal cycles of HOA (grey symbols), black carbon apportioned to traffic emissions eBC_{ff} (dashed lines) and NO_x (dotted lines) for weekdays (a) and weekends (b). The shaded areas represent interquartile range for 1-hour average HOA.

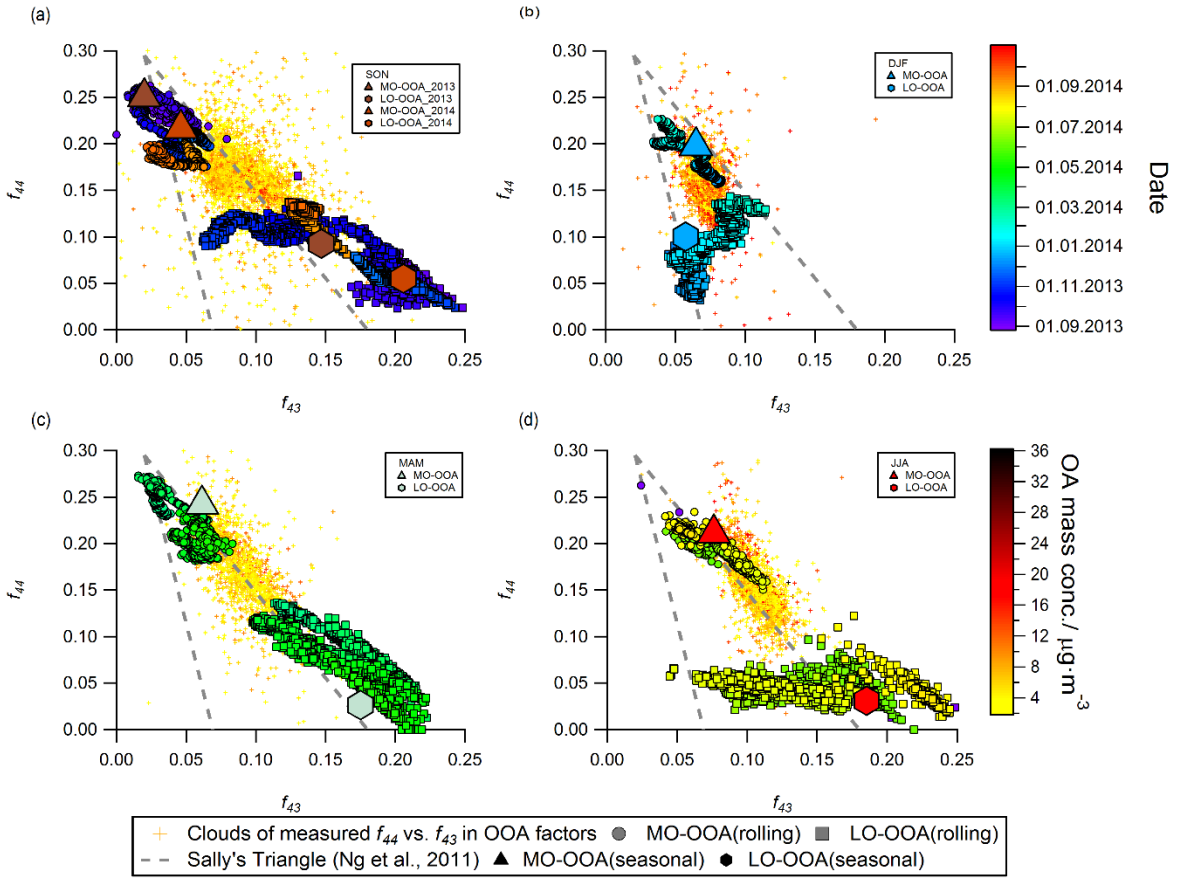

Fig. 7 OOA f_{44} and f_{43} for four different seasons. The yellow cloud of data points represents the f_{44} vs f_{43} by subtracting the f_{44} and f_{43} contributed from HOA, BBOA and LOA factors. They are color coded by the total OA mass concentration. The circles, triangles, and squares

represent the ratio between f_{44} and f_{43} intensities within the factor profiles of MO-OOA and LO-OOA, respectively. While the smaller size of circles, triangles, and squares are from rolling PMF analysis, which are color coded by the date and time. The dash line are the Sally's triangle from (Ng et al., 2011) and depicts the region where several PMF-OOA from the last decade resided in the f_{44} vs f_{43} space.

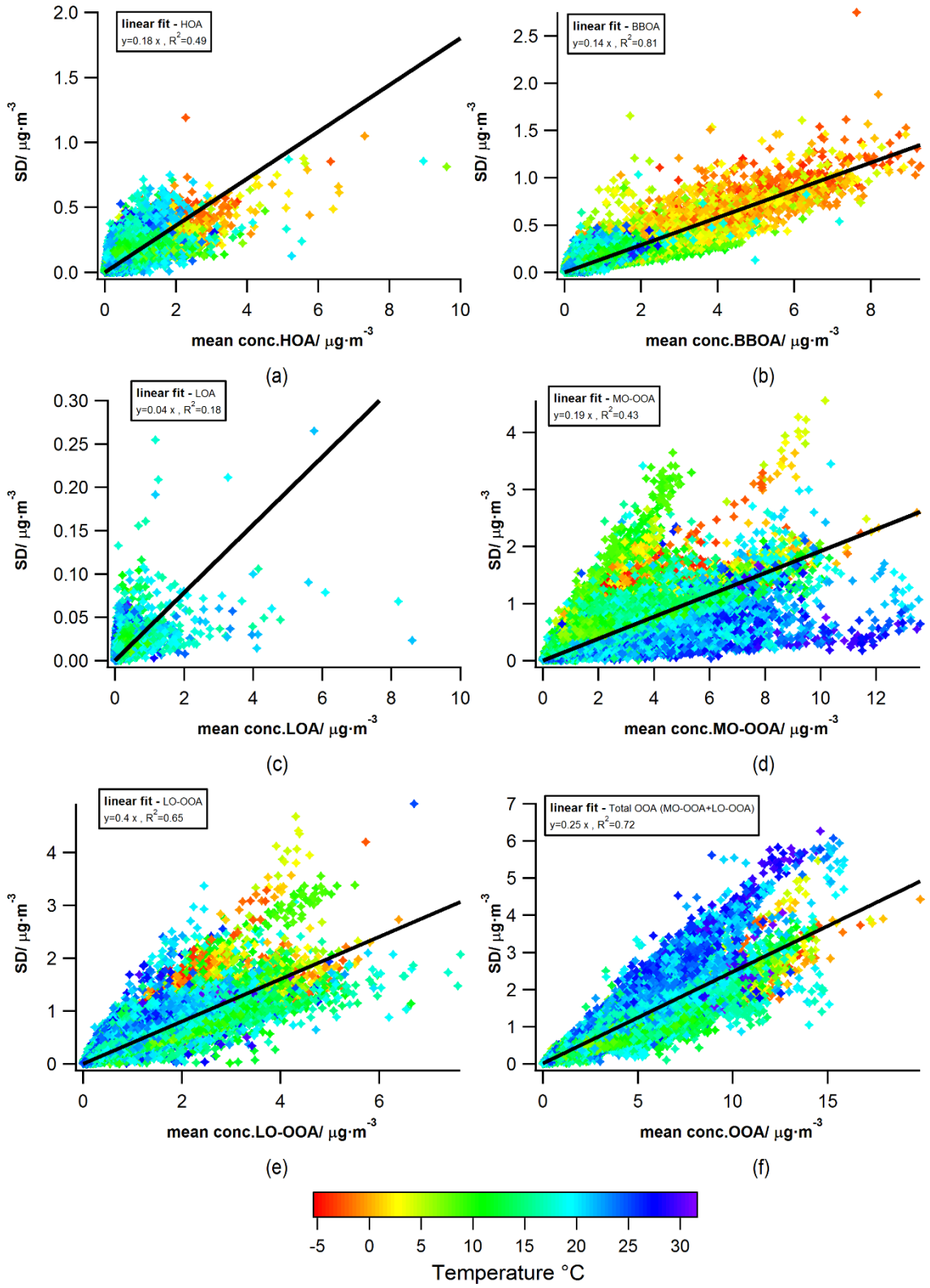

Fig. 8 Absolute statistical uncertainties of PMF for HOA, BBOA, LOA, LO-OOA, MO-OOA and total OOA (LO-OOA+MO-OOA) for all data. The data points colour-coded all data points

~~by temperature. The PMF error (uncertainties) of selected PMF runs and rotational uncertainties is estimated using the slope of the linear regression of standard deviation (σ) vs. the averaged mass concentration (μ) for each factor.~~

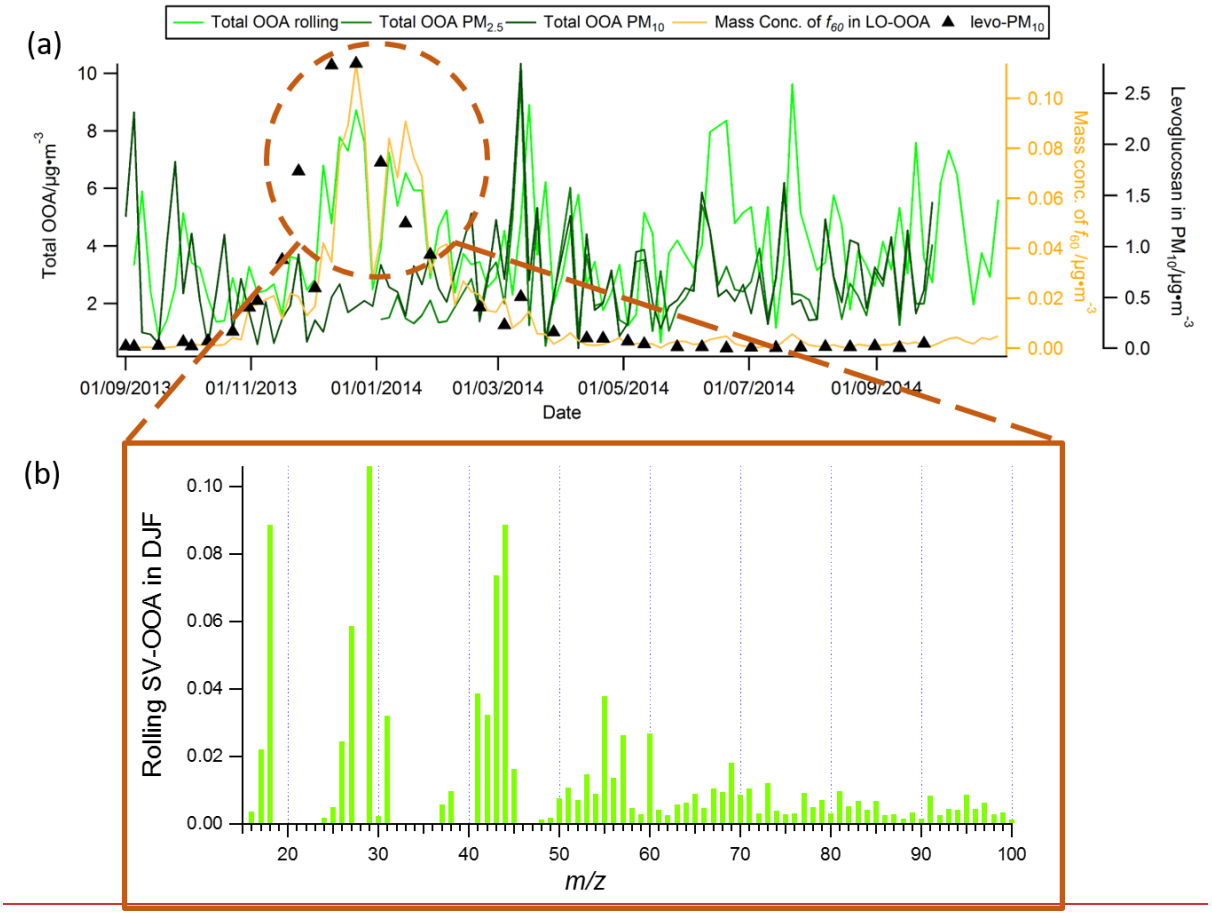

~~Fig. 9~~ ~~(a) Time series of total oxygenated organic aerosol (LO-OOA+MO-OOA) from online and offline source apportionment solutions, together with f60 in LO-OOA for online solution, and levoglucosan in PM10 filter; (b) Averaged LO-OOA factor profile from online solution during DJF (Dec, Jan, and Feb), when online total OOA is significantly higher than that of offline solutions.~~